ADDIS ABABA UNIVERSITY

ADDIS ABABA INSTITUTE OF TECHNOLOGY

SCHOOL OF MECHANICAL AND INDUSTRIAL ENGINEERING
MECHANICAL DESIGN (MSC)

DESIGN AND ANALYSIS OF ELECTROMAGNETIC BRAKING SYSTEM FOR LIGHTWEIGHT VEHICLE

BY

HARNET TEKLE

A THESIS SUBMITTED TO THE SCHOOL OF GRADUATE STUDIES OF ADDIS ABABA UNIVERSITY IN PARTIAL FULFILLMENT OF THE REQUIREMENTS FOR THE DEGREE OF MASTERS OF SCIENCE IN MECHANICAL ENGINEERING
(MECHANICAL DESIGN STREAM)

ADVISOR: DANIEL T. REDDA(Ph.D.)

JANUARY 26, 2024

ADDIS ABABA INSTITUTE OF TECHNOLOGY

SCHOOL OF MECHANICAL AND INDUSTRIAL ENGINEERING

MECHANICAL DESIGN (MSC)

DESIGN AND ANALYSIS OF ELECTROMAGNETIC BRAKING SYSTEM FOR LIGHTWEIGHT VEHICLE

BY

HARNET TEKLE

The undersigned have examined the thesis entitled 'Design and Analysis of an Electromatically Braking System for LightWeight Vehicle' presented by **Harnet Tekle**, a candidate for the degree of **Master of Science,** and hereby certify that it is worthy of acceptance.

Dr.Daniel T Redda Advisor	_____	_____
_____ (Internal Examiners)	_____ Signature	_____ Date
_____ (External Examiners)	_____ Signature	_____ Date
_____ (Dean of Schools')	_____ Signature	_____ Date
_____ Chairperson	_____ Signature	_____ Date

ADDIS ABABA INSTITUTE OF TECHNOLOGY

SCHOOL OF MECHANICAL AND INDUSTRIAL ENGINEERING

MECHANICAL DESIGN (MSC)

DESIGN AND ANALYSIS OF ELECTROMAGNETIC BRAKING SYSTEM FOR LIGHTWEIGHT VEHICLE

BY

HARNET TEKLE

Undertaking

I hereby declare that the research work titled "Design and Analysis of Electromagnetic Braking System for LightWeight Vehicle" is my work. The work has not been presented elsewhere for assessment. Where material has been used from other sources it has been properly acknowledged/referred.

_____ _____

Harnet Tekle Date

This is to certify that the above declaration made by the candidate is correct to the best of my knowledge.

_____ _____

Dr. Daniel T. Redda (Advisor) Date

Acknowledgment

I would like to express my sincere gratitude to my supervisor **Dr. Daniel T. Redda** for his support throughout my thesis project. I am thankful for his scientific guidance, his constructive criticism and friendly advice. But above all, I am grateful to him for sharing his illuminating views and his solid way of thinking on several issues. Also, I am thankful to my family for their numerous support in my life choices. Finally, I like to share my gratitude to Lifan Motors for their collaboration in data collecting.

Abstract

In this study, an optimized electromagnetic brake system (EMB) is designed and simulated to replace the conventional hydraulic brake (CHB) system of a lightweight vehicle Lifan 530. The electromagnetic brake system is a pure frictionless electromechanically controlled actuator that has the potential to further reduce braking time and braking distance. The primary goal of this research is to design an electromagnetic braking system that replaces the CHB of the Lifan 530 car to stop as a standalone using a 12v battery source. A theoretical and numerical model is developed in the quarter vehicle model. Using ANSYS Workbench 2020 R2, a 3D finite element model of the EMB was created by SpaceClaim 2020 R2 to simulate and optimize the EMB domain using magnetostatic analysis to study the magnetic flux and braking torque created by the system. Steady-state thermal analysis was performed to investigate heat buildup and the thermal effect of the electromagnet on the brake system. In addition, a static structural analysis is performed to investigate the structural response to temperature changes. The finite element (FEM) has been used to optimize the magnetic circuit design for maximizing the braking torque. The optimized electromagnetic result is achieved by using a wire diameter of 3.2×10^{-4}m and 70 turns. Which results in a maximum torque of $338\ Nm$ The simulated result revealed that the braking torque increases with the conducting area and shows the suitability of the concept for the selected vehicle in terms of dynamics, installation space, and energy requirements without demanding extra battery. Finally to validate the numerical result MatLab and ANSYS software are utilized.

Keywords: Brake, Conventional hydraulic brake, Electromagnetic brake, Eddy current, Finite element.

Contents

List of Figures

List of Table

Nomenclature

A_f	Vehicle frontal area
A_{core}	Magnetic core area
$A_{airgap1,2}$	Area of the air gap
$A_{winding}$	Area of winding
B	Magnetic flux density
C_d	Aerodynamic drag coefficient
Cp	Specific heat capacity
C_r	Rolling friction coefficient
D	Circumscribed circle diameter
E	Electric field intensity
F_{zf}	Front reaction force
F_{zr}	Rear reaction force
F_f	Friction force
F_n	Normal force
F_z	Transfer of weight
F_{aero}	Aerodynamic resistance force
H	Magnetic field intensity
I	Effective inertia
I_w	Wheel inertia
I_e	Engine inertia
J	Current density
L	Inductance
L_{base}	Wheelbase
L_f	The length from the center of the wheel to the center of gravity
L_r	The length from the center of gravity to the center of the rear wheel
N	Number of turns

P	Power
P_c	Core loss
P_E	Eddy current loss
P_H	Hysteresis loss
Q	Heat transferred
R	Resistance
R_w	Wheel radius
R_x	Rolling resistance force
$\mathcal{R}_{\text{core}}$	The reluctance of the core
$\mathcal{R}_{\text{airgap1,2}}$	The reluctance of the first and second airgap
$\mathcal{R}_{\text{cond}}$	Conducting disk reluctance
T_b	Braking torque,
T_d	Driver torque
T_e	Engine torque
T_l	Engine load torque
T_a	Ambient temperature
T_{max}	Maximum temperature
ΔT	Temperature difference
U_e	Input electrical energy
U_f	Co magnetic energy
U_m	Mechanical energy
V	Velocity
V_{vol}	Volume
V_x	Longitudinal vehicle velocity
$\dot{V}_x$	Longitudinal vehicle acceleration
W_v	Vehicle weight

d	Disk thickness
d_{wire}	Wire diameter
g	Gravity
h	Heat transfer coefficient
h_{cg}	Center of gravity
h_a	Aerodynamics height
k	Thermal conductivity
l_{core}	Core length
l_{window}	Window length
l_{wire}	Mean turn length
m_v	Vehicle mass
m_t	Quarter vehicle mass
m_w	Wheel mass
t	Time
v	Voltage
w_H	The outer hysteresis loop area
φ	Gear ratio
α_w	Wheel angular acceleration
α_e	Engine angular acceleration
$\mathcal{E}$	Electromotive force
ε	Emissivity
θ	Angle
$\ddot{\Theta}$	Angular acceleration
λ	The slip
μ	Permeability
μ_f	Friction coefficient

μ_0	Permeability of the air
μ_r	Relative permeability
ρ	Density
ρCp	Thermal mass
$\boldsymbol{\sigma}$	Conductivity
σ	Stefan-Boltzmann constant
Φ	Magnetic flux
ω	Angular velocity
ω_w	Wheel angular velocity
ω_e	Engine angular velocity

Abbreviations

CHB Conventional Hydraulic braking system

EBD Electronic Brake-Force Distribution

EMB Electromagnetic braking system

EMF Electromotive force

ESP Electronic Stability Program

FeSi Iron silicon

MPL Magnetic path length

MRB Magnetorheological Brake

MRF Magnetorheological Fluid

PPA Pole Projection Area

SR Switched Reluctance

TCS Traction Control System

Chapter one

1. Introduction

1.1. Background of study

Technology intended to enable automobiles to accelerate faster and achieve faster speeds has developed with an ardor that is only seen in the aviation sector in the little over a century since the invention of the vehicle captured the public's imagination. Because of physics or technological constraints, a land-based vehicle cannot travel faster than certain limits. About the largely hidden aspect of automotive evolution, the same cannot be stated [1]. Robust braking and quicker reaction times are essential components of an automated highway system's overall automated control [2]. The only restrictions placed on them have to do with how quickly the human body can decelerate. Otherwise, stopping a car would be much simpler than getting it moving quickly [1].

There is a continuous further development of the brake system in a motor vehicle. For example, recent innovations, including electronic stability program ESP, traction control system TCS, electronic brake-force distribution EBD [3], and so on which resulted in further growth of active safety. but this is not always efficient due to the reason computers may fail to read those programs so a permanent solution for the brake system instead of adding programs to the conventional system.

A change to a new braking system is required to move toward green technology, which emphasizes the value of environmental conservation. A new braking system that replaces the existing one that employs the brake pad would help lessen the noise pollution (squeal and noise) and air pollution that comes with using a conventional braking system [4]. Debris from brake wear is a possible environmental risk. Numerous dangerous substances included in wear debris have the potential to interact with living things' DNA and cause cancer [5]. In addition, copper from worn brake pads enters rainwater and streams that feed San Francisco Bay, hurting fish and destroying algae and crustaceans. The auxiliary hydraulic parts of the conventional brake system, including the master cylinder, booster, transfer lines, and brake actuators, contribute to its large size and weight [6].

Besides its environmental and weight disadvantage the conventional system has economic problems such as brake pad wear due to friction this requires continuous maintenance which is

costly and make drivers fade up go to the garage, and the brake fluid can face the problem of vaporization and freezing though to stabilize this problem were forced to use ant-freeze volatile agents (additives) It made the system more expensive and complex [7].

Regarding performance, CHB has numerous disadvantages, including poor braking performance at high speeds and thermal degradation brought on by contact movement, doesn't resistance to high temperatures as a result of brake fading, the problems of time delay in pressure building up, air and water in the hydraulic system and brake fluid leakage can cause a problem on the efficiency of braking by system delay in response or the system may not work at all in emergency condition and lead as to suffer in an accident [8].

Realizing the importance of a new brake system the popularity of magnetic braking has risen significantly in the last several years. Since its introduction in 1987, magnetic braking has found many practical applications, and it is still widely used in the industry today [9]. This occurrence has applications in the separation of nonmagnetic metals from solid waste, damping of undesired nutation in satellites, and elimination of vibration in spacecraft [10]. On heavy vehicles, electromagnetic brakes are currently utilized in addition to conventional friction brakes as additional retardation equipment [11]. To support the hydraulic braking system, Desta created an eddy current braking device that was installed on the vehicle's transmission axle. Anwar and Zheng created a nonlinear sliding-mode-type controller for slip regulation in a braking event and talked about the antilock-braking algorithm for an eddy current-based brake-by-wire system. Gay demonstrated a contactless magnetic brake for use in automobiles; Song evaluated the performance of a hybrid electric brake system with a sliding mode controller; and Gay described in his papers an integrated mechanism based on electromagnetic and hydraulic braking. To assess the braking performance, a mathematical model and a hybrid system configuration known as HEBS were developed. created a composited braking system using a conventional hydraulic braking system and an eddy current braking system as the foundation. The composited brake system shortened the stopping distance, as demonstrated by the findings of the testing [12]. As the next generation of brake-by-wire technology, companies like Continental Automotive Systems and Delphi Corp. have been heavily involved in the development of commercially accessible EMBs. These are intended for use in passenger cars with traditional powertrains as well as those with cutting-edge power sources, such as advanced battery-electric, fuel cell, and hybrid electric propulsion [13]. A

switching reluctance SR motor, for instance, has been suggested by Delphi as a potential actuation technique for EMB applications [13]. The pads in these systems are squeezed onto the revolving disk utilizing switching reluctance SR motors. SR motors are more appealing to brake applications because of their high-temperature operation capabilities, robustness, dynamic bandwidth, and fail tolerance even if permanent magnet DC motors are more efficient, controllable, and economical [14]. The magnetorheological brake (MRB) is the next segment of the EMB. The magnetorheological fluids (MRF) used in these brakes change viscosity in response to an applied magnetic field. The MRF fills in the space between the brake's stator and rotor, and by actively adjusting the fluid's viscosity through the external magnetic field, the brake produces variable shear stress, which acts as a retarding force. [13].

The friction brakes can be utilized less frequently and seldom ever get hot by using the electromagnetic brake as additional retardation equipment. Brake linings have a significantly longer lifespan before needing repair, and brake fade issues are potentially prevented. According to studies done by a truck manufacturer, the electromagnetic brake performed 80% of the work that the standard service brake would have been expected to do. However, the electromagnetic brake eliminates the risks associated with using friction brakes excessively beyond their capacity to release heat. This is most likely to happen when a car is traveling quickly down a lengthy grade. An electromagnetic brake is relatively easy to install. It doesn't require an additional cooling system. It does not affect the engine's efficiency. Additionally, the electromagnetic brake is more controllable. Using the heat energy's convection and radiation at high temperatures, the electromagnetic brakes are made thermally stable. Excellent heat dissipation efficiency is possessed by the electromagnetic brakes. The thermal dynamic performance of electromagnetic brakes is superior to that of conventional friction brakes [8].

The electromagnet brake system provides a better response time for emergencies and is safer, with no heat loss, frictionless, longer-lasting, more robust, and requiring less service. Better performance at a lower cost and weight is provided by electromagnetic brakes, which is what's needed today. These brakes' numerous benefits make them a great substitute for traditional brakes. To replace the traditional brake system on a light car, an optimal electromagnetic brake system is created and simulated in the thesis work. The electromagnetic brake system is an entirely

frictionless electromechanically operated actuator that can potentially cut down on both the vehicle's and the brake system's weight. It can also shorten the stopping distance.

1.2. Problem statement

Towards green technology, which focuses on the importance of environment conservation, a transition to a new braking system is needed. A new braking system to replace the current braking system which uses the brake pad will help to reduce the air pollution and noise pollution (noise and squeal) that happen while using a conventional braking system. Brake wear debris represents a potential hazard to the environment [4]. Wear debris contains several hazardous elements that may interact with the DNA of living organisms and cause carcinogenesis [5]. Besides that, copper from brake pad wear also finds its way into stormwater and tributaries feeding into San Francisco Bay, killing invertebrates and algae and harming fish [6].

The conventional brake system is also bulky in size and heavy weight due to its auxiliary hydraulic components such as the master cylinder, booster, transfer lines, and brake actuators. Besides its environmental and weight disadvantages the conventional system has economic problems such as brake pad wear due to friction this requires continuous maintenance which is costly and makes drivers fade up to go to the garage, and the brake fluid can face the problem of vaporization and freezing though to stabilize this problem we forced to use ant-freeze and ant-volatile agents (additives) which increases the complexity and cost of the system [7]. Regarding performance CHB has many drawbacks such as thermal failure due to its contact movement, poor braking performance at high speed doesn’t resist high temperatures resulting in brake fading, the problems of time delay in pressure building up, air and water in the hydraulic system and brake fluid leakage can cause a problem on the efficiency of braking by system delay in response or the system may not work at all in emergency condition and lead as to suffer in an accident [8].

Realizing the importance of a new braking system that could lead to environmentally friendly and reduce common problems mentioned, there are ongoing attempts to replace CHB and researchers have shown that electromagnetic brakes are efficient in many ways. However, its realization of EMB as a standalone device for automotive use is yet to emerge and there are still gaps that should be filled to apply for a lightweight vehicle control system. For instance, the electromagnetic braking system's performance in a heavy vehicle demonstrates how the battery is depleted considerably more quickly when the brake system is powered by the battery and perhaps an

additional battery will be required to power the electromagnetic coil when high brake torque is required [15], the poor ability at low speed is also a limitation to the practical application [16] . Prior research has looked at ways to increase performance without taking the material and structure of the electromagnets into account.

1.3. Objective

1.3.1. General Objective

The main objective of this thesis is to design and analyze a full Electromagnetic brake system for a lightweight vehicle that will replace the conventional braking system and act as a standalone braking system for the Lifan 530 car using a 12v battery source.

1.3.2. Specific Objective

- To determine the braking torque using mechanical modeling and determine the electromagnetic specifications using electrical modeling
- To develop a modeling and simulation on finite analysis using ANSYS software
- To carry out magnetostatic analysis to determine and optimize the flux distribution and torque created by the EMB system
- To analyze the temperature and stress distribution on disk created due to magnetization
- Perform result validation using ANSYS and MATLAB software

1.4. Scope of The Study

This work intends to contribute to the design and analysis of an optimized electromagnetic braking system EMB for a lightweight vehicle in substitution of a conventional hydraulic braking system CHB. This work only focuses on theoretical and mathematical analysis and verifies the design outputs by simulation using ANSYS and MATLAB software.

1.5. Significance of the Study

The purpose of the study is to deliver a substitute system for the conventional hydraulic braking system of a lightweight vehicle. substituting the hydraulic system with an electromechanical system can provide an environmental advantage and shorter braking time which leads to a shorter braking distance. besides enhancing the braking system to shorter time braking to save more lives

from danger during accidental braking. Furthermore, this study provides recommendations for future studies.

1.6. Limitation of the Study

Since the area of this study is new, limited works of literature are available which made the study difficult to access standard input parameters, formulas, and literature-supported assumptions.

1.7. Organization of the Study

There are five primary sections to this thesis study. The first chapter serves as an introduction, outlining the context of the investigation, the issue statement, the goal of the study, its limitations, its scope, and its importance. The review of the literature is the second chapter, and it discusses terms of design considerations, methodology, and material selections that have been used in previous works in electromagnetic study areas. The third chapter is about numerical and analytical methods and conditions, in this chapter, the electromagnetic braking system is designed and states procedures and conditions for the simulation and optimization process. The fourth chapter is the result and discussion in this part the output simulation results are discussed and compared with the mathematical modeling. Finally, in the fifth chapter which is the conclusion and future work in this final portion of the study the entire work is summarized and concluded based on the findings from the previous chapters, and at the end, the work for future study is recommended under the topic of future work.

Chapter Two

2. Literature Review

2.1. Material Selection

In the design of electromagnetic brake systems, material selection is critical. The magnetic circuit, as well as the structural and thermal properties, are significantly influenced by the materials employed in EMB. Consequently, a material with strong mechanical qualities, high electrical conductivity, and adequate power dissipation capabilities is required because EMB depends on a variety of material features.

2.1.1. Conducting Disc

The material used for the conducting disc is crucial, and it must have strong mechanical qualities, high electrical conductivity, and enough power dissipation capabilities.

Prof. N.B.Totala [11] developed the electromagnetic braking system as a supplementary retarder to guarantee the driver, passenger, and other road users' comfort and safety. A steel disk is drawn to the coil or solenoid in his proposed electromagnetic brake. Between itself and a stationary steel disc, the steel disc presses a brake disc composed of asbestos or sintered material. Disc material for electromagnetic braking should have to have nonmagnetic characteristics to be a good conductor therefore steel cannot satisfy be conducting disc for the electromagnetic braking system due to the reason steel is a ferromagnetic material and has small thermal conductivity.

M. Talaat and N.H. Mostafa [17] explored a technique for analyzing the eddy current in the unique scenario of a rotating copper disk in a time-variant field. According to their findings, there is a noticeable decrease in current density and the angular velocity of the rotating disc nearly stops at 25 seconds for flux densities of 1 T and 7 seconds for 2 T. The induced magnetic flux, which lowers the net magnetic flux passing through the magnetic pole, is responsible for the decrease in the eddy current density value. Even though it is common to use copper for disc material because is excellent in electric and thermal conductivity copper is expensive, difficult to machine, heavy, harder, has low tensile strength with repeated bending, and low contact resistance when oxides are not present compared to Aluminum.

M.Z Baharom and Gigih Priyandoko [18] conducted an experiment on eddy current braking to review the behavior of three different materials with a thickness of 1mm with 200mm of diameter utilized as disc brake, which is copper, aluminum, and Zink. From their experimental result, Aluminum exhibits the greatest deceleration when utilized as the disc brake for electromagnetic eddy current braking when compared to copper and zinc.

Besides, new material must be designed or selected for the brake disc that improves the weight of the brake system, good thermal properties, and fast reaction of braking like Aluminum and other alloys. In this work, aluminum is selected as conducting material.

2.1.2. Magnetic Core

The magnet core, an essential part of a vehicle's electromagnetic braking system, is designed with material selection playing a major role. It is essential for producing the magnetic field that causes the rotating conducting disc to experience eddy currents. The eddy current braking system's overall efficacy, performance, and efficiency are impacted by the selection of materials for the core magnet.

Prof. N.B.Totala [11] developed the electromagnetic braking system as a supplementary retarder to guarantee the driver, passenger, and other road users' comfort and safety. He used a soft iron core as a core magnet However, iron can lose its magnetic property after a finite temperature, which reaches saturation point (Curie temperature of iron is 770^{o}C).

Ren He and Xuejun Liu [12] To address issues with standard car brake systems including wear, heat failure, and delayed reaction, an eddy current and electro-hydraulic hybrid brake system should be implemented. They converted the wheel's kinetic energy into electrical using a permanent magnet generator so that the eddy current brake could be powered. However, permanent magnets can be used if the field does not have to be adjusted frequently it can come quickly to the original position after demagnetization.

Karakoc [13] proposed the magnetorheological brake MRB for a small vehicle the brake consists of an enclosed electromagnet and many revolving disks submerged in a magnetorheological fluid. The magnetorheological fluids (MRF) used in these brakes change viscosity in response to an applied magnetic field. By regulating the external magnetic field, the MRF actively modifies the fluid viscosity and bridges the gap between the brake's stator and rotor. low carbon steel, although

plastic deformation affects the magnetic characteristics of low carbon steels, AISI 1018 was chosen as the magnetic material in the magnetic circuit due to considerations of cost, permeability, and availability.

One of the disadvantages of using steel in the past was that losses would rise with the material's age. Therefore, it is important to come up with an idea that improves the problem using other alternative alloys of ferromagnetic materials like silicon steel and low carbon steel, which are soft materials to have low magnetic hysteresis and high saturation point to keep the performance of the magnetic brake.

The benefits of adding silicon to steel were twofold: it enhanced the material's durability over time and raised electrical resistivity, which decreased eddy current losses. High flux density saturation, relatively good permeability at high flux density, and a mild loss at audio frequency are all provided by silicon steel. A significant advancement in silicon steel was achieved by the cold-rolled, grain-oriented technique AISI type M6. This M6 grain-oriented steel has a high permeability and very low losses. Because it is used in applications that demand great performance, there won't be many losses. One of the earliest alloys used in transformers and inductors was silicon steel. It has significantly improved over time and is likely the most extensively used magnetic substance when weighed pound for pound [19].

2.1.3. Magnetic Wire

The magnetic field that interacts with the conductive material in the brake system is created by the electromagnetic coil. To increase the magnetic field's intensity, the coil's material should have a high magnetic permeability.

The most common electromagnetic device's magnetic coils are wound with copper magnet wire. [13] [11] [17] [18]. There are numerous insulation options for copper magnet wire, but polyimide varnish, which can withstand temperatures up to 450°F (230°C), is the highest temperature insulation. Depending on the specific application, this wire is usually utilized in sizes ranging from 20AWG to 35AWG. For copper magnet wires in this size range, stainless steel-clad copper wire with ceramic fiber insulation is the most widely available higher-temperature substitute. The purpose of this specific type of wire was to be used in thermocouples and high-temperature sensors. It is rated and available for use at temperatures up to 1300^{o}F (700^{o}C). Although this sort of wire has a rather large minimum bend radius because of the ceramic insulation, it is not a drop-in

replacement for normal copper magnet wire. This kind of wire cannot be electrically connected using conventional methods like soldering because of the stainless-steel cladding. Instead, welding is required. Copper wire and permanent magnets, two common materials used to create electromagnetic devices, cannot function at temperatures beyond 1000 degrees Fahrenheit (500 degrees Celsius) [20].

In this work, Aluminum silicon is used to substitute the conventional copper wire due to its flexibility and ability to handle higher temperatures.

2.2. Method and Conditions

The majority of research studies demonstrate that electromagnetic problems are analyzed using analytical techniques and the finite element approach.

Lee and Park [21] point out improving the braking torque generation of the ECB at low velocity by using a sinusoidal field. Using numerical methods, the braking torque generation was examined on a configuration with three PPAs, and the applied field's frequency was tuned to improve the braking torque generation. A laminated magnetic core was used to remove the induction effects. Although only Lee and Park's study addressed the possibility that an AC-based magnetic field application could further expand the capacity for braking torque production, no prior research has looked into the specific application of such a field for resolving the braking torque constraint of an ECB at low speeds.

Karakoc [13]considered the application of a time-varying magnetic field and the lowering of torque at low speeds. An unsymmetrical multifrontal approach, an effective direct solver for non-symmetric geometry, is used to solve the resulting problem. The FEM solution is used to compute the braking torque. Additionally, by applying time-varying fields of various shapes at constant and varied frequencies, the optimal brake torque capacity is found using this model. The governing linear Maxwell's equations are used by Karakoc for the problem under consideration. Thus, using the formula he suggests to compute the braking torque, the outcome demonstrated that using FM as opposed to DC field braking can result in a 60% increase in braking torque. However, the system requires wide space to install and continuous maintenance.

Li Luo et al [22] acquaint with a three-dimensional finite element simulation method that fully accounts for the penetration depth and marginal effect. They compared the electromagnetic braking

torques obtained using the conventional algorithm and finite element simulation. The integrated electromagnetic auxiliary disc brake device for motor vehicles is intended to supplement conventional braking. They calculated the eddy current and magnetic field distribution on the disc based on assumptions. Their Findings indicate that at both medium and high speeds, the braking action is effective. However, they failed to consider material considerations and most of the parameters are assumptions.

The insufficiencies of the analytical model are addressed in this work through numerical analysis. The effects of geometric, electrical, and magnetic properties are investigated to determine the optimal shape and material properties for the electromagnetic brake. Numerical modeling also yields a conceptual design and testbed for automotive applications. Furthermore, the required part design is completed by relating the mechanical and electrical analyses to the design of the electromagnetic brake system parts. A Proper material selection is made, the vehicle quarter model is developed to calculate the braking torque, and Ampere’s law and Faraday's law are applied to calculate the magnetic field parameters. ANSYS software is used for system simulation and optimization when employing the 3D finite element method.

Chapter three

3. Numerical and Analytical Methods and Conditions

3.1. Material Selection

In designing an electromagnetic brake material selection is an important phase. The criteria in the selection process vary depending on the application, strength, availability, machining, price, and Corrosion would be taken into consideration. In terms of performance, the electromechanical characteristics of the material are the first consideration is always. Therefore, the issues for the material selection are discussed in terms of:

I. Magnetic properties
II. Structural properties
III. Thermal properties

I. Magnetic Properties

The magnetic properties of materials influence the design of apparatuses. permeability μ is the main parameter that defines the magnetic characteristics of the material. Permeability is the ratio of the applied magnetic field intensity H and magnetic flux density B because of the intensity through the material. The material is able to transfer magnetic flux over itself. relative permeability μ_r, which is the ratio of the permeability of the material and the permeability of a vacuum which is $\mu_0 = 4\pi\ 10^{-7}$ H/m [19].

Most of the materials that are magnetic are metallic, and metals conduct electric currents. when the magnetic field changes in the material eddy currents are produced, which produce an opposing magnetic field. The magnetic field in the metallic material is the sum of the magnetic field generated by the magnetizing coil minus the field generated by the electric current flowing in the magnet to oppose this field.

II. Structural Properties:

Automotive manufacturers are always looking for ways to make their cars look better, weigh less, be stronger, and perform better in collisions. It is a crucial challenge, though, to strike a balance between a material's strength, stiffness, resistance to dimensional tolerances, and appearance and

feel. Materials are more important than ever for automakers and suppliers. The selection of materials affects the price, danger, safety, weight, market perception, and vehicle missions.

Weight reduction in the automotive industry can be obtained in three ways [23]:

- Replacing materials of high specific weight with lower density materials without reducing rigidity and durability (for example replacement of steel with aluminum, magnesium, composites, and foams)
- Optimizing the design of load-carrying elements and exterior attachments to reduce their weight without any loss in rigidity or functionality; and,
- Optimizing the production process

III. Thermal properties:

The braking system works by changing the kinetic energy into thermal energy therefore thermal characteristics of a material play a vital part in the design of the braking system. Hence, the rotating disc is where the majority of the heat transfer occurs. Therefore, high thermal conductivity k, specific heat capacity Cp, density ρ , and thermal mass ρCp to facilitate heat flow and absorption for good thermal performance, although to accommodate in the design of vehicle suspensions there has to be a consideration between brake thermal mass and the unsprung mass. By surface convection and radiation, the heat is transferred into and through the rotating disc and is dissipated to the surrounding air. Therefore, the material for the brake disc has to be good for cooling by radiation and the high coefficients of surface heat transfer associated with forced convection from the airflow over the disc.

The capacity of a metal to conduct heat is measured by its thermal conductivity. This characteristic varies depending on the kind of metal and should be considered in applications where high operating temperatures are typical including for the material that is used for electromagnetic coil. Thermal conductivity in pure metals increases with temperature almost exactly. On the other hand, the thermal conductivity of alloys rises with temperature.

3.1.1. Material Selection for Disc Brake

The brake system for the lightweight vehicle is four wheels controlled by disc brakes as shown in Figure 3.1 which feature better heat dissipation, smaller thermal attenuation in both high temperature and water soaking and more excellent braking effect with a reduced tendency for pull

than drum brake. The most important thing about a disc brake is the cooling ability and ease of maintenance hence major components are exposed to air.

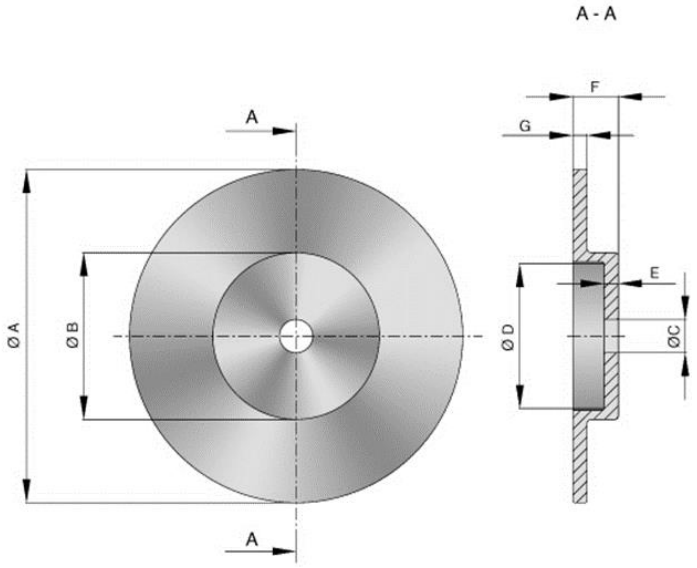

Figure 3.1 Figure Schematic representation of disk brake

Achieving minimizing consumption of fuel as well as emissions of greenhouse gas is a current issue in automotive industries. Since the brake disc or rotor is a vital device from the point of view of safety, under varying loading conditions, velocity, thermal, and environment, materials related to brake systems should have steady and consistent characteristics and high durability. when selecting a brake disc material there are numerous factors to be considered. the ability of the brake disc material to have high thermal conductivity as well as it have to has nonmagnetic characterstic are the most important considerations. Other requirements during the design phase are weight, manufacturing processability, and cost. In order to prevent distortion or fracture due to thermal stress until the heat is released, the brake disc needs to have an adequate thermal storage capacity.

Conductor materials that are most commonly used for the construction of normal conduction are aluminum and copper. Both materials are available in different grades and purities. Aluminum (Al) is the best material for electromagnetic brake discs due to its good conductivity, lightweights, and other benefits. Aluminum is the second most used material in the auto industry next to steel. It is believed that one kilogram of aluminum could replace up to two kilograms of steel or cast iron in the manufacturing process. Aluminum has superior structural properties and is very light its density is one-third (10%-40% lighter) that of steel which saves 0.7 gallons of fuel per 100 miles, a saving of 15 % in fuel consumption over steel vehicles [24], and is extremely malleable which allows

desired shape optimized for maximum performance. Aluminum is excellent in conducting heat and electricity, has high strength with tensile strength ranging from 70-700Mpa, and most importantly aluminum is a nonmagnetic material. Also, it has environmental benefits using aluminum auto manufacturing gives a 20 % smaller lifecycle CO_2 footprint compared to using steel, and nearly 90% of automotive aluminum scrap is recovered and recycled. These properties make it ideal for a wide variety of uses, from construction to cooking utensils to auto manufacturing [24].

3.1.2. Material Selection for Magnetic Core

Magnetic cores for several types of modern electrical and electronic devices require magnetic materials with many combinations of characteristics and properties. The most important factor in the design of magnetic components is the magnetic material. Electrical steels are the most commonly used type of soft magnetic core material. In this thesis work, silicon steel is chosen as the magnetic core material it is a soft material to has low magnetic hysteresis and a high saturation point to keep the performance of the magnetic brake.

Silicon steel is a soft magnetic material that is used in electrical power transformers, motors, and generators [19]. Because of their low carbon content, a more fitting metallurgical name for these materials would be iron silicon alloy. However, the term electrical steels has been universally accepted as the designation for flat-rolled magnetic materials in which silicon is the principal alloying element. Their electrical and magnetic characteristics make them suited for laminated cores where the flux reverses direction or pulsates many times each second. In practice, electrical steels are divided into several general classes [25]. They are created according to the material's fundamental magnetic property, form, differences from the majority of grades, or production process.

Of the four general classes, one is Non-oriented, these are electrical steels, in which the magnetic properties are practically the same in any direction of magnetization in the plane of the material. The term non-oriented is used to differentiate these materials from those produced by processes that create a definite orientation or directionality of magnetic properties. And the second one is Grain-oriented, this term is used to designate electrical steels that possess magnetic properties, which are strongly oriented concerning the direction of rolling. A process of rolling and annealing can produce alloys of a suitable composition with a metallic crystal structure in which the grains are aligned so that magnetic properties are vastly superior in the direction of rolling. This results

in inferior properties in other directions, However. Well, the third one is Fully processed, which is electrical steel, whose magnetic properties are completely developed by the steel producer. The name is derived from the fact that the materials are completely processed, and ready for use without any additional processing required to achieve the desired magnetic quality. However, a low-temperature heat treatment may be employed by the user to eliminate stresses introduced by the fabrication of the material into cores. and the other fourth one is Semi-processed, these electrical steels, which are finished to final thickness and physical form sheets or coils by the producer but not fully annealed to develop final magnetic quality. With these materials, the achievement of magnetic properties by the annealing treatment becomes the responsibility of the user. Due to the intricacies of developing adequate magnetic properties, grain-oriented steels are produced fully processed [25].

Grain-oriented silicon steel is used for non-rotating applications, i.e. transformers, which are characterized by a strong preferred crystallographic orientation. The reason for the intensive demand for grain-oriented steel was the remarkable opportunity these steels afforded to reduce the size of magnetic cores in electrical apparatus, thereby also reducing the number of other materials required. Related factors that expanded the application of this class of electrical steel include Permeability at high flux densities is improved while core loss is reduced. This is in contrast to the improvement of nonoriented grades where core loss improvements usually are accompanied by lower permeability at high flux densities. Power production and transmission economy warrant the design of a more efficient apparatus using better core materials [19]. With grain-oriented steel, the cost of the core generally is not increased, even though the price per unit weight of core material is higher. oriented steel cores are decidedly smaller than those of the same rating made of conventional silicon steel [25].

The magnetic properties of electrical steel are especially sensitive to stress. Substantial reductions in magnetic properties can be caused by the stress of only a few hundred kilograms per square meter which would, of course, produce an elastic strain. Likewise, stresses that produce plastic deformation of electrical steel create even greater changes in the magnetic properties. These changes occur because the metal crystals in the strained metal are distorted. This distortion of the crystal or atomic structure affects the relationship between magnetizing force and induction and consequently affects all the magnetization characteristics of the material. Normally, stresses create

a harmful effect by causing the degradation of magnetic properties. since the silicon content of nonoriented low core loss grades is high, ultimate strength, yield point, and shear strength will generally be greater than higher core loss grades with lower silicon content. Therefore, if the silicon is much lower, eddy-current loss and, as a result, the core loss in the desired thickness will be too high. If silicon content is much higher, the metal has poor ductility. High silicon content also reduces saturation density, therefore requiring a higher exciting current at high flux density and limiting the operating induction [25].

Hysteresis loss and eddy current loss decrease with increasing silicon content from 0.21 to 2.0 wt%. The reduction in hysteresis loss was mainly due to texture and grain size, and the reduction in eddy current loss was primarily due to the increase in resistivity. Usually, oriented iron-silicon alloys contain approximately 3.0 to 3.5% silicon. The electrical resistivity of 3% silicon iron is approximately 48 micro-ohms-cm (1 $\Omega m 10^{-8}$). This is about five times higher than low-carbon steel. Saturation magnetization is reduced by the presence of silicon, dropping by about 6% with 3% Si. The use of the material above 3.2% Si is limited by the difficulty in rolling it to a thin strip for laminations [26].

Silicon steel 3.2 wt%Si is currently the most popular choice for motors and transformers because it offers balanced electrical and magnetic properties, and perhaps more importantly, low cost. It is composed of silicon and iron, two of the earth's most abundant elements. Besides, the conventional 3.2 wt% silicon steel has excellent ductility, allowing the slabs coming out from the continuous casting line to be directly hot-rolled into hot bands with 3 to 5 mm thickness, then cold-rolled into thin laminates of less than 1 mm thickness [27].

Therefore, for this thesis work, the silicon content of about 3.2 % (mass percentages) is selected as the magnetic core of the system due to its better electrical resistivity and eddy current losses reduction therefore minimizing magnetic losses.

Moreover Iron silicon (Fe-Si) steel 3.2 % as a core magnet is superior in saturation temperature than iron core which is 900^0c Curie temperature and high relative permeability, one.

3.1.3. Material Selection for Magnetic Coil

According to the screw rule, the magnetic flux lines surround the conductor in the existence of electric current in a winding form of a solenoid as shown in Figure 3.2 similar to a permanent magnet magnetic field is formed.

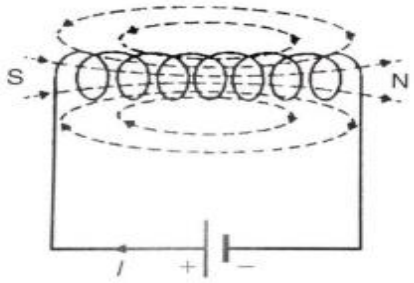

Figure 3.2: induced magnetic field in a solenoid

In electromagnetism solenoid is important. the current inside a solenoid is important for inducing a magnetic field and for its magnitude, by controlling the current flow the magnetic field can be regulated. Therefore, by making a resistance wire we can control the amount of current in a circuit.

To design the electromagnetic coil the capacity of receiving a few hundred to several thousand amperes, withstanding a few hundred to several thousand volts, and mechanical forces caused by the electrical current flow must be taken into consideration. As well as generating the required magnitude of the magnetic field to magnetize the material, inducing sufficient duration of a magnetic field pulse to let fully saturate the magnetic field, having an adequate cooling system so that the needed production cycle rates can happen and during in contact for operation must be safe. The safety matters must also consider physical forces and electrical voltages.

In this case, when choosing the material for a magnetic coil, corrosion resistance, temperature coefficient of resistivity, and resistor stability are often the most important factors. A high-resistivity alloy is desirable.

Aluminum was a good alternative in the past since it was much cheaper, nowadays copper coils are more state-of-the-art. Nevertheless, pure aluminum is usually too soft to be drawn into a fine wire. Therefore, aluminum is usually alloyed with 1% Si or 1% Mg to produce a strengthening mechanism. At ambient temperature, 1% silicon exceeds the solubility of silicon in aluminum by a factor of fifty, which results in silicon precipitation. the amount and therefore the size of the

silicon precipitates are hooked into the cooling rate from higher temperatures. Slower cooling rates end in more precipitation and enormous nonuniform silicon nodules, while faster cooling rates don't allow sufficient time for silicon precipitation leading to uniformly dispersed nodules. Silicon grain size can affect wire ductility, and the second phase can become a possible nucleation site for fatigue cracks [28].

In this work, Aluminum alloy with 1% silicon (AlSi) is used as an electromagnetic material due to its specific electrical and magnetic properties that are relevant for eddy current applications. AlSi has low magnetic permeability. This property is desirable in eddy current applications to minimize magnetic losses and the efficiency of the system can be maintained. The resistivity of AlSi is higher compared to pure copper, which means if an electric current passes through it may produce more heat. This can be a factor to consider in eddy current applications where heat generation needs to be managed. Compared to conventional copper wire AlSi has lower melting points and is less heat-resistant, has good corrosion resistance, is lightweight, and has minimal cost than copper.

3.2. Dimension

Table 3.1 Input Data were taken from Lifan-530

Vehicle specification		
Drive Type		FWD
Dimension parameter	$LxWxH$	4700x1765x1490mm
Wheelbase	L_{base}	2.55m
Tread front/rear	$b_{f/r}$	1465/1460mm
Ground clearance		172mm
Front/rear suspension		810/940mm
Min turning radius		4.8m
Brake disc thickness	D	0.0205m
Wheel radius	R_w	0.1235m
Curb mass	m_v	1140kg
Cross weight	m_{tv}	1515 kg
Wheel mass	Mw	8.5 kg
Engine specification		
Type		4 stroke p
Cylinder		4
Volume		1.5L
Max. power/rev	P	76kw/6000rpm
Max. engine torque/rpm	T_e	119Nm/4000rpm
Top vehicle speed	V	170km/h

3.3. Methods and Conditions

3.3.1. Theoretical Analysis

The theoretical modeling delivers a piece of primary critical information about the sensitivity to design parameters and sizing of the brake. The working principle of the electromagnet is when the driver presses the brake pedal represented as 2 in Figure 3.3 unlocks the controlling switch represented as 3 to energize the electromagnetic barking EMB shown as 4 from the battery voltage represented as 1 to hold the braking disc 5 from rotation. When the driver releases the braking pedal the controlling switch closes the circuit from allowing the voltage to enter the circuit, therefore, disabling the battery from energizing the electromagnetic braking system.

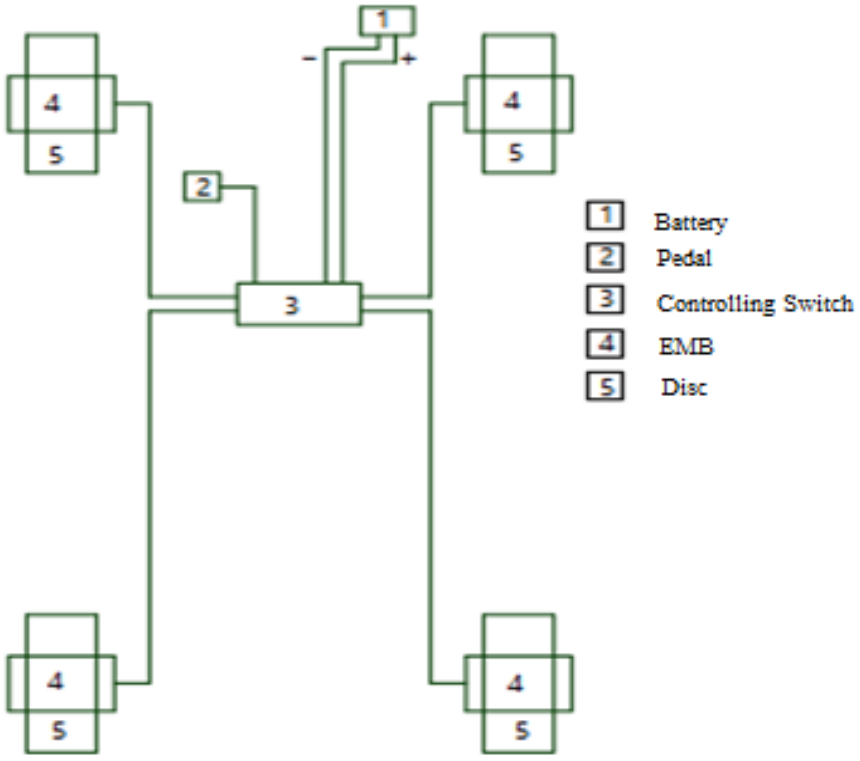

Figure 3.3: vehicle electromagnetic brake system configuration

3.3.1.1 Theoretical Modeling of Electromagnet

In this thesis work, an electromagnet contactless brake system is proposed to overcome the problems of the conventional hydraulic brake and provides a system that can replace the CHB as a standalone system. Therefore, an analysis of the distribution of the density of eddy current as well as the braking torque for a rotating disc that has a finite radius is presented.

The model is considered for simulation as a three-dimensional field problem to analyze the eddy-current in conducting disc as well the induced magnetic and electric fields. the magnetic and electric fields are computed accurately hence they are a prerequisite for induced eddy current to be determined through the calculation. A Finite Element Method (FEM) is used to study the eddy current distribution in the rotating conductive disc. The disc material is considered linear, and nonmagnetic. The solution for the problem can then be taken by the superposition of two sub-problems: an eddy-current problem and a static problem. it is assumed that no stator magnetization, only eddy currents in the disc for the eddy-current problem, and only the stator magnetization is considered there are no eddy currents in the static problem.

3.3.1.2 Structural Modeling

Three regions are divided by geometry the disc is bounded by airgaps on both sides of the disc. As a region of infinite permeability employing a boundary condition for the air gap Figure 3.4 shows the pole is modeled into regions of the decomposition of the geometry, where the air-gap width is designated as $l_{air\ gap}$ and the thickness of the disc is d.

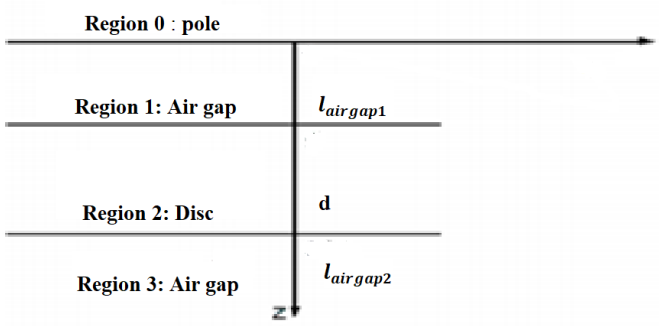

Figure 3.4: Two-dimensional regions

3.3.2. Numerical Modeling

To overcome the limitations of the analytical model a numerical analysis was used. The effect of magnetic, electrical, thermal, and geometric parameters was studied for the eddy-current brake to determine the optimum geometry and material properties. This modeling is used to design a testbed and deliver a conceptual design for applications in automotive as well.

3.3.2.1. Vehicle Dynamics (Mechanical Modeling)

A typical mathematical model is assumed for vehicle dynamics and control study. This particular vehicle model includes two steerable wheels up front and two steerable wheels along the back that are attached to a rigid body. This model had to figure out how much braking torque a brake should have. Longitudinal forces, aerodynamic drag forces, rolling resistance forces, and gravitational forces all affect the dynamics of the vehicle. As seen in Figure 3.5, the coordinate system is fixed to the vehicle, with the origin located at the center of gravity of the vehicle and the x, y, and z axes oriented longitudinally, laterally, and vertically, respectively.

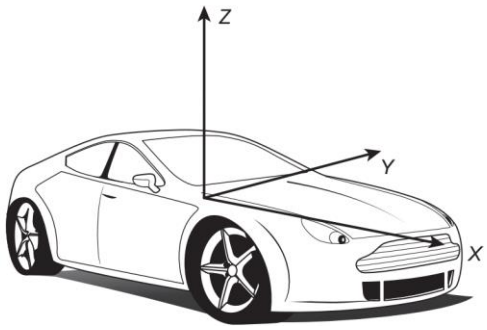

Figure 3.5: Vehicle coordinate system(ISO)

The vehicle motion has six independent degrees of freedom with this coordinate system, such as Longitudinal motion in the x-direction, rolling motion around the x-axis, pitching motion around the y-axis, left and right movement in the y-direction, yawing motion around the z-axis and vertical motion in the z-direction.

To calculate the center of gravity of the vehicle it has to be at static conditions by considering the vehicle as a structural beam which is reinforced at both ends by a roller that has reactions F_{zf} and F_{zr}. However, the total vehicle weight is specified at the center of gravity represented in Figure 3.6. at which the vehicle body is centered at the center of gravity.

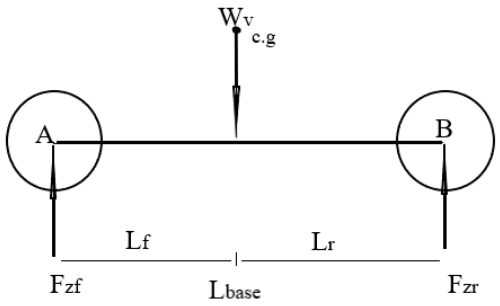

Figure 3.6: Representation of vehicle as a beam

According to DE Alembert's law summations of all forces in the same direction is zero,

$$\sum F_Y = 0 = F_{zf} + F_{zr} - W_v \quad \ldots\ldots 3.1$$

Assume Moment in the counterclockwise direction is positive,

$$\sum M_B = 0 = W_v \times L_r - F_{zf} \times L_{base} \quad \ldots\ldots 3.2$$

Solving for the length from the center of gravity to the midpoint of the rear wheel L_r ,

$$L_r = \frac{F_{zf} L_{base}}{W_v} \quad \ldots\ldots 3.3$$

$$Hence,\ L_{base} = L_f + L_r \quad \ldots\ldots 3.4$$

Therefore, Equation 3.3 is substituted into Equation 3.4 and solved for the length from the center of the front wheel to the center of gravity L_f:

$$L_f = L_{base} - \frac{F_{zf} L_{base}}{W_v} \quad \ldots\ldots 3.5$$

There are two options to determine the center of gravity's height h_{cg} those are the lifting method and the tilting method. Therefore, raising (Lifting) the vehicle's front axle for about 1000 mm height and shifting the total vehicle into the rear axle is shown below in Figure 3.7.

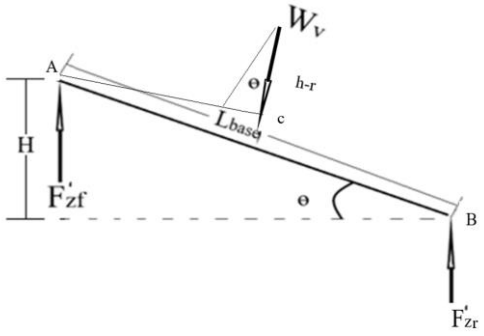

Figure 3.7: Lifted front axle of the vehicle

Assume Moment in the counterclockwise direction is positive,

$$\sum M_A = 0 = F'_{zr} L_{base} \cos\theta - W_v \times AC \quad \ldots\ldots\ldots\ldots\ldots\ldots\ldots\ldots 3.6$$

Where the length AC from trigonometric relation,

$$AC = (h_{cg} - R_W) \times \sin\theta + L_f \cos\theta \quad \ldots\ldots\ldots\ldots\ldots\ldots\ldots\ldots 3.7$$

From trigonometry the angle θ,

$$\theta = \sin^{-1}\frac{H}{L_{base}} \quad \ldots\ldots\ldots\ldots\ldots\ldots\ldots\ldots\ldots\ldots\ldots\ldots 3.8$$

$$\theta = \sin^{-1}\frac{1}{2.55} = 23^{O}$$

Subsite Equation 3.7 into Equation 3.6 and solve for h_{cg}

$$h_{cg} = \frac{(F'_{zr} - F_{zr})}{W_v} \times L_{base} \times \cot\theta + R_W \quad \ldots\ldots\ldots\ldots\ldots\ldots\ldots 3.9$$

$$h_{cg} = \left(\frac{1394.5N - 774.5\,N}{1515kg\,x\,9.81\,m/s^2}\right) x2.550\,m\,x\,\cot 23^{O} + 0.1235m$$

$$h_{cg} = 0.37\text{m}$$

I. Quarter Vehicle Dynamics

This model's fundamental assumption is that the vehicle's mass is distributed evenly among its four wheels.

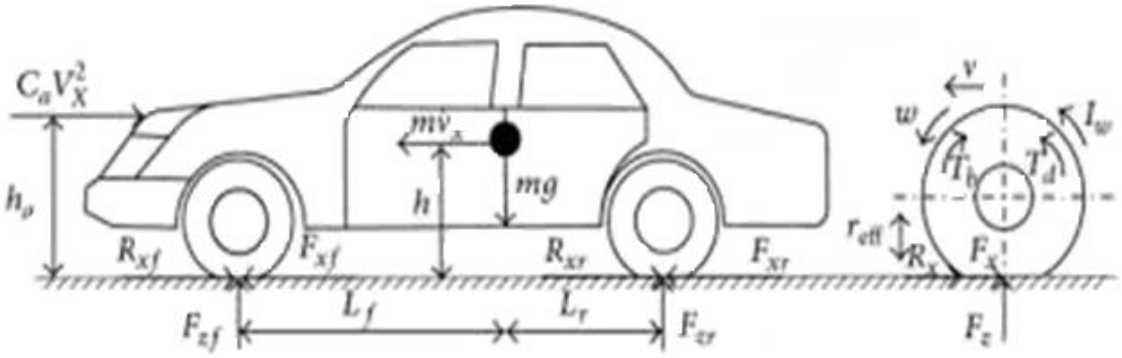

Figure 3.8: longitudinal vehicle dynamics

Considering the counterclockwise moments as positive and the summation of moments on the rear wheel is zero from the above Figure 3.8. therefore, the vertical load F_{zf} can be found

$$\sum M = -m_v g L_r - F_{zf} L_{base} - m_v \dot{V}_x h_{cg} - F_a h_a = 0 \quad \ldots\ldots 3.10$$

$$F_{zf} = \frac{-m_v g L_r - m_v \dot{V}_x h_{cg} - F_a h_a}{L_{base}} \quad \ldots\ldots 3.11$$

A free body diagram in Figure 3.9 shows a counter-clockwise rotating wheel during braking, the brake, T_b, applies torque, and aerodynamic resistance force F_a, rolling resistance force R_x, friction force F_f, normal force F_n, and the transfer of weight F_z caused by braking of the vehicle. the total mass moment of inertia I and the vehicle's angular acceleration $\ddot{o}$. The wheel radius of the is R_w and the vehicle traveled distance x.

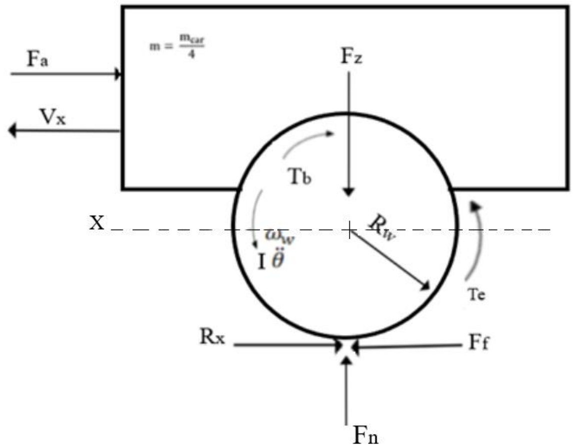

Figure 3.9: Schematic representation of vehicle dynamics quarter model

In the case of deacceleration, the balanced force along the longitudinal axis of the vehicle is:

$$m_t\dot{V}_x = F_f - R_x - F_{aero} \quad \text{……………………………… 3.12}$$

Given the vehicle quarter model, the amount of mass carried by the single wheel is found by the summation of the cross-vehicle mass's quarter and the wheel mass:

$$m_t = \frac{1}{4}m_v + m_w \quad \text{……………………………………… 3.13}$$

m_v stands for the mass of the vehicle and m_w is the wheel mass and from Table 3.1 are 1515kg and 8.5kg respectively.

$$m_t = \frac{1}{4}x1515\ kg + 8.5\ kg$$

$$m_t = 387.25kg$$

According to Newton's second law, the corresponding aerodynamic drag force that acts on the vehicle can be denoted as:

$$F_{aero} = \frac{1}{2}\rho C_d A_f {V_x}^2 \quad \text{…………………………………… 3.14}$$

The aerodynamic force acts on the vehicle is the product of the mass density of air ρ, the aerodynamic drag coefficient C_d, the frontal area of the vehicle A_f, which is the projected area of the vehicle in the direction of travel, and the square of the longitudinal vehicle velocityV_x.

Atmospheric conditions affect air density ρ and hence can significantly affect aerodynamic drag. The commonly used standard set of conditions to which all aerodynamic test data are referred is a

temperature of 15 ° C and a barometric pressure of 101.32 kPa. The corresponding mass density of air ρ may be taken as 1.225 kg / m^3 [29].

The frontal area A_f is in the range of 79-84 % of the area calculated from the vehicle width and height for passenger cars according to Wang from Theory of Ground Vehicles [29], the following relationship between vehicle mass and frontal area can be used for passenger cars with a mass in the range of 800-2000 kg:

$$A_f = 1.6 + 0.00056(M_v - 765) \quad \text{3.15}$$

$$A_f = 1.6 + 0.00056(1515 - 765)$$

$$A_f = 2.02\ m^2$$

Therefore, the equivalent aerodynamic drag force on a vehicle is

$$F_{aero} = \frac{1}{2} x\ 1.225\ kg\ /\ m^3\ x\ 0.26\ x 2.02\ m^2\ x(47.2\ m/s)^2$$

$$F_{aero} = 716.7\text{N}$$

According to de 'Alembert theorem, the summations' of all vertical force are zero,

$$\sum F_y = 0 = F_n - F_z - m_t g \quad \text{3.16}$$

$$F_n = F_z + m_t g \quad \text{3.17}$$

Substitute Equation 3.11into the Equation 3.17 and solve for F_n

$$F_n = m_t g - \left(\frac{m_v g L_r + m_v \dot{V}_x h_{cg} + F_a h_a}{L_{base}}\right) \quad \text{3.18}$$

Where the wheelbase L_{base} and the center of gravity's height $h_{cg}$and aerodynamics height h_a which is equal in magnitude to the center of gravity for passenger cars.

The amount of deacceleration needed to stop the vehicle at 2.5 seconds from moving at 170km/h or 47.2 m/s velocity to stop;

$$\dot{V}_x = \frac{dV_x}{dt} \quad \text{3.19}$$

$$\dot{V}_x = -\frac{47.2 m/s}{2.5 sec} = -19\ m/s^2$$

Therefore, the normal force acting on the wheel from Equation 3.18 is

$$F_n = m_t g - \left(\frac{m_v g L_r + m_v \dot{V}_x h_{cg} + F_a h_a}{L_{base}}\right)$$

$$F_n = 387.25\ kg x\ 9.8\ m/s^2 - \left(\frac{1515kg\ x\ 9.8\ m/s^2 x\ 1.275m + 1515kg\ x\ (-19m/s^2)\ x\ 0.37\ m + 716.7\ N\ x\ 0.37\ m}{2.55m}\right)$$

$$F_n = 444N$$

The frictional force up on the wheel is well-defined about the normal force and the coefficient of friction between the tire and the surface, and the force against the motion of the wheel is defined as rolling resistance:

$$R_x = C_r F_n \ldots\ldots\ldots\ldots\ldots\ldots\ldots\ldots\ldots\ldots\ldots\ldots\ldots\ldots\ldots\ldots. \; 3.20$$

The coefficient of rolling friction $C_r$in the function of speed can be found:

$$C_r = 0.01(1 + \frac{V}{147}) = \ldots\ldots\ldots\ldots\ldots\ldots\ldots\ldots\ldots\ldots\ldots\ldots \; 3.21$$

$$C_r = 0.01\left(1 + \frac{170}{147}\right)$$

$$C_r = 0.021$$

Therefore, the rolling resistance R_x is found by substituting the result of C_r from Equation 3.21 to 3.20:

$$R_x = C_r F_n = 0.021\ x\ 444N = 9.3N$$

The force of friction and normal force are directly proportional to each

$$F_f = \mu_f F_n \ldots\ldots\ldots\ldots\ldots\ldots\ldots\ldots\ldots\ldots\ldots\ldots\ldots \; 3.22$$

Where during braking the coefficient friction is μ_f is defined as in function of the slip ratio λ and the slip ratio λ is

$$\lambda = \frac{R_W \omega_W - V_x}{V_x} \ldots\ldots\ldots\ldots\ldots\ldots\ldots\ldots\ldots\ldots\ldots\ldots\ldots \; 3.23$$

$$\lambda = \frac{0.1235m\ x 309\ rad/s - 47.2\,m/s}{47.2\,m/s}$$

$$\lambda = 0.2$$

Where ω_w is the wheel's angular velocity, *Graph 1* (Appendix II) is illustrated to show the correlation between the slip ratio and the friction coefficient for different types of surfaces the coefficient of friction μ_f is read from the graph as one for dray asphalt.

Therefore, the friction force is found as equal to the normal force.

$$F_f = 1x444\ \mathrm{N}$$

$$F_f = 444\ N$$

From Newton's second law in an acceleration phase, the forces acting on the wheel allow the expression of rotational and longitudinal dynamics main equations. Therefore, wheel rotational dynamics can be found by applying the equilibrium moment equation on the wheel axis of rotation.

$$I\alpha_w = T_d - T_b - R_w F_f + R_w R_x \quad \ldots\ldots\ldots\ldots\ldots\ldots\ldots\ldots\ldots\ldots \quad 3.24$$

where $\alpha_w$is the wheel's angular acceleration, wheel radius R_w of the, T_d is driver torque, I is effective inertia and T_b is the braking torque of the wheel,

The expression for the effective mass moment of inertia is the summation of the inertia of the wheel I_w and engine inertia I_e on the wheel, where φ is the gear ratio which is taken from Appendix I *Table 0.5*:

$$I = I_w + \frac{1}{\varphi^2} I_e \ldots\ldots\ldots\ldots\ldots\ldots\ldots\ldots\ldots\ldots\ldots\ldots\ldots\ldots \quad 3.25$$

The moment of inertia on the wheel is

$$I_w = \frac{1}{2} m_w {R_w}^2 \ldots\ldots\ldots\ldots\ldots\ldots\ldots\ldots\ldots\ldots\ldots\ldots\ldots \quad 3.26$$

$$I_w = \frac{1}{2} 8.5\ kg\ x\ (0.1235m)^2$$

$$I_w = 0.065 kgm^2$$

Engine inertia is calculated at the maximum rpm of the engine that produces maximum torque,

$$I_e = \frac{T_e - T_l}{\alpha_e} \ldots\ldots\ldots\ldots\ldots\ldots\ldots\ldots\ldots\ldots\ldots\ldots\ldots \quad 3.27$$

Where T_e is engine torque, T_l engine load torque after loss and is α_e is the angular acceleration of the engine and it can be found as the differential of the engine's angular speed. Therefore, by substation of Equations 3.24 and 3.25 to Equation 3.22 the effective inertia can be calculated.

The engine load torque can be considered as

$$T_l = -6.7644\ x10^{-3} {\omega_e}^2 + 28.8\ x\ 10^{-3} {\omega_e}^2 - 20.4477\ x\ 10^{-3} {\omega_e}^2 \ldots\ldots\ldots\ldots \quad 3.28$$

$$T_l = -6.7644\ x10^{-3} x 418.9^{\,2} + 28.8\ x\ 10^{-3}\ x\ 418.9^{\,2} - 20.4477\ x\ 10^{-3} x\ 418.9^{\,2}$$

$$T_l = -6.1\text{x}10^{-6}\ \text{Nm}$$

The engine acceleration is a time derivative of the angular velocity where the angular speed to generate high torque is 4000rpm from Table 3.1.

$$\omega_e = \frac{2\,x\pi x n_e}{60} = \frac{2\,x\,\pi\,x\,4000rpm}{60} = 418\,rad/s$$

Therefore, the angular acceleration,

$$\alpha_e = \frac{\omega_e}{t} = \frac{419\ rad/s}{2.5\,sec} = 167.6\,rad/s^2$$

Solve for engine inertia,

$$I_e = \frac{T_e - T_l}{\alpha_e} = \frac{119\,Nm - (-6.1\,x\,10^{-6})Nm}{167.6\,rad/s^2} =$$

$$I_e = 0.7kg\,m^2$$

The equivalent effective mass inertia is

$$I = I_w + \frac{1}{\varphi^2} I_e$$

$$I = 0.065\,kg\,m^2 + \frac{0.7kgm^2}{0.738^2}$$

$$I = 1.35kg\,m^2$$

Finally, solve for braking torque Equation 3.24,

$$I\alpha_w = T_d - R_w F_f + R_w R_r - T_b$$

$$(1.35kg\,m^2\,x - 154\,rad/s^2) = 119\,Nm - (0.1235m\,x\,444N) + (0.1235m\,x\,9.3\,N) - T_b$$

$$T_b = 273Nm$$

Therefore the total amount of braking torque required to stop the vehicle is found from this mechanical modeling as 273 Nm.

3.3.2.2 Electrical Model of Brake

A rotating conductive disk experiences an induced eddy current when magnetic flux flows through it Figure 3.10 (b) in Figure. Eddy current and magnetic flux interact to provide a retarding braking force. As seen in Figure 3.10 (a) a magnet brake's most basic design consists of an electromagnet and a conductive disc. The disc rotates while the magnet produces a constant magnetic flux. A moving conductor in the presence of a magnetic flux creates currents, and the currents' Lorentz forces cause the disc to slow down.

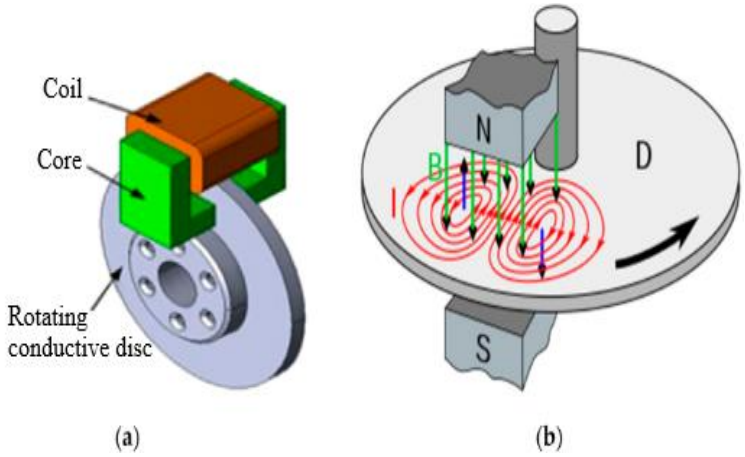

Figure 3.10: Schematic representation of (a) electromagnetic brake system (b) rotating passing through a magnetic field

According to Faraday's disc theory, a conducting disc is rotated around its axis with angular velocity ω, so a part of the disc at distance r from the axis moves at a velocity equal to $\omega r\hat{\phi}$ in a magnetic field parallel to the axis is,

$$V\ x\ B = B\ x\ \omega r\ \hat{r} \quad \ldots\ldots\ldots\ldots\ldots\ldots\ldots\ldots\ldots\ldots\ldots\ldots\ldots\ldots\ldots\ldots\ 3.29$$

So, if one electrode is attached to the disc's axis and the other electrode to a brush sliding along the disc's rim, electromotive force EMF is found as integral at differential radius,

$$\varepsilon = \int_{axis}^{rim} B\omega r\ \hat{r} \cdot \vec{dl} = \int_{0}^{radius} B\omega r dr \quad \ldots\ldots\ldots\ldots\ldots\ldots\ldots\ldots\ 3.30$$

For a uniform magnetic field across the disc, this integral can be simplified as,

$$\varepsilon = B\ x\ \omega\ x \frac{r^2}{2} \quad \ldots\ldots\ldots\ldots\ldots\ldots\ldots\ldots\ldots\ldots\ldots\ldots\ldots\ldots\ 3.31$$

The above Equation 3.31 demonstrates in Figure 3.11 that an electromagnet, or stationary source of magnetic flux, is the foundation of an eddy-current brake, with a moving conductor, or conducting disc, in front of it.

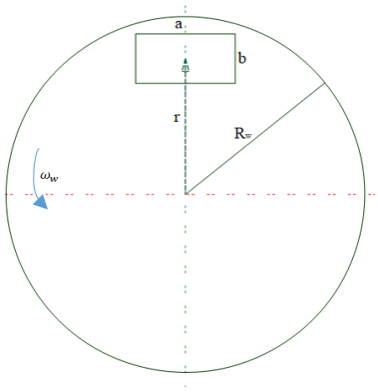

Figure 3.11: magnetic core cross-section

The motion causes a time-varying magnetic flux density in the conductor, which Lenz's law states produces an electric field.

$$\nabla \times \vec{E} = \frac{\partial \vec{B}}{\partial t} \quad \ldots\ldots 3.32$$

According to Ohm's law, this electric field causes currents to circulate in the conductor,

$$\vec{J} = \sigma . \vec{E} \quad \ldots\ldots 3.33$$

These currents are called “eddy currents”, where J is current density, E electric field intensity, and σ the eddy-currents and flux density interaction create a force that opposes the motion:

$$\vec{F} = \vec{J} \times \vec{B} \quad \ldots\ldots 3.34$$

The induced external field is the multiplication of the force generated by the field and the radius of the wheel generates a torque,

$$T_b = \vec{F} \times r = \vec{J} \times \vec{B} \times R_w \quad \ldots\ldots 3.35$$

Maxwell’s vector equation can be rewritten as

$$T_b = \int_v \vec{J} \times \vec{B} \times R_w dv \quad \ldots\ldots 3.36$$

The torque produced by the eddy currents can be calculated by integrating the currents over the cylindrical volume of the disc that is covered by the magnet pole, assuming that the magnetic flux is uniform through the air gap and that the conductive disc fits precisely within the air gap.

Finally, the simplified form of the integral is:

$$T_b = \frac{\pi}{4}\sigma D^2 dB^2 {R_w}^2 \omega_w \ldots\ldots\ldots\ldots\ldots\ldots\ldots\ldots\ldots\ldots\ldots\ldots\ldots\ldots\ldots\ldots 3.37$$

Where is the specific conductivity of the material σ, the diameter of the circumscribed circle for the magnet core D, the thickness of the disk d, magnetic field B assumed to be constant throughout the airgap, wheel radius R_w, and instantaneous angular velocityω_w represented in Figure 3.11 diagrammatically.

I. Design of Magnetic Core

In electrical, electromechanical, and magnetic devices like electromagnets, generators, electric motors, transformers, inductors, magnetic recording heads, and magnetic assemblies, a magnetic core is a section of magnetic material with a high magnetic permeability that is used to confine and guide magnetic fields. The core material has to have a higher permeability than the surrounding air, which causes the magnetic field lines to concentrate on it. To produce the magnetic field, a wire coil that carries current is often wrapped around the core. The main purpose of any magnetic core is to give flux a convenient route so that it can allow flux linkage, also known as coupling, between two or more magnetic elements. By joining a magnetic source with a magnetic load, it functions as a magnetic bus bar.

The magnetic core design consists of a crossectional area as illustrated in Figure 3.12 that exposes the length and direction of magnetic flux in which the current and magnetic field path. Therefore, the core crossectional area can be calculated from the mechanical modeling driving from the torque equation.

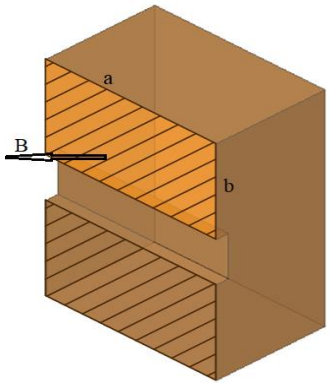

Figure 3.12: Cross-sectional area of the magnetic core perpendicular to the magnetic field

Driving the formula for the core magnet diameter from the toque equation above Equation 3.37,

$$T_b = \frac{\pi}{4}\sigma D^2 d B^2 {R_w}^2 \omega_w$$

$$D^2 = \frac{4T_b}{\pi\sigma d B^2 {R_w}^2 \omega_w} \quad \text{.....3.38}$$

The thickness of the disk can be found from the moment of the inertia of a wheel Equation 3.26. Where ρ is the density of the material, the density of the aluminum disk is a standard 2712 kg/m^3.

$$I_w = \frac{1}{2} m_w {R_w}^2 = \frac{1}{2}\rho d\pi {R_w}^4 \quad \text{.....3.39}$$

$$0.065\, kg/m^2 = \frac{1}{2} x\ 2712\ \ kg/m^3\, x\pi x (0.1235m)^4 x d$$

$$d = 0.0205m$$

From Equation 3.38, the calculated value of conducting disk thickness d is 0.0205m by substituting the standard and calculated parameters. To find the D the B and the specific conductivity are taken standard from the datasheet *Graph 2* (Appendix II). The magnetic flux density of grain-oriented electrical steels reaches the saturation point from 1.5T up to 2 T.

Hence, the application of this design is for the small weight (purpose) relative to the transformer and electrical induction motors the B should be lower to reduce the core loss, and noise produced by the magnetic field can be reduced by less magnetostriction. Therefore, magnetic flux B for iron silicon steel core is selected 0.15T. where the specific conductivity σ of aluminum is 3.5x10^7 s/m is taken as a standard value from the datasheet.

By substituting the above values into Equation 3.37,

$$D^2 = \frac{273\ Nm\ x\ 4}{\pi x 3.5\text{x}10^{\,7}\ s/m\ x\ (0.15\, Wb/m)^2\ x\ 0.0205m\ x (0.1235m)^2\ x\ 382\, rad/s}$$

$$D = \sqrt{\frac{273 Nm\ x\ 4}{\pi x 3.5\text{x}10^{\,7}\ s/m\ x\ 0.0205m\ x\ (0.15\, Wb/m)^2\ (0.1235m)^2\ x\ 382\, rad/s}}$$

$$D = 0.0608m$$

The magnetic core protection in Figure 3.12 shows rectangular-like cross-section cores are suitable for small voltage. the two edges of the core, a and b are different in dimension as shown in the figure. the diameter of the circumscribing circle is diagonal to the core.

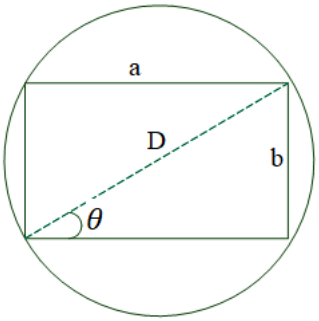

Figure 3.13: Cross-section of rectangular core

As illustrated in Figure 3.13, the depth a and height b of the magnetic core cross-section can be calculated using sine-cosine rue, from geometric relation θ is 30°.

For the depth a,

$$cos\,\theta = \frac{a}{D} \quad \text{.....3.40}$$

$$a = D\cos 30° = 0.0608mx\ \cos 30°$$

$$a = 0.053m$$

For height b,

$$sin\,\theta = \frac{b}{D} \quad \text{.....3.41}$$

$$b = D\sin\theta = 0.0608m\ x\ \sin 30°$$

$$b = 0.030m$$

Therefore, the area of the magnetic cross-section A_{core} is the output multiplication of the width and depth of the core cross-section.

$$A_{core} = a\ x\ b \quad \text{.....3.42}$$

$$A_{core} = 0.053mx\ 0.030m$$

$$A_{core} = 0.0016m^2$$

Iron loss (core loss) P_c is one of the most important properties of soft magnetic materials. Iron loss is the energy loss (in watt/ kilogram or watt/pound) per cycle at a specific frequency and flux density [30]. *Table 0.6* (appendix I), the iron loss of iron silicon FeSi 3.2 wt% silicon is expressed in terms of a watt per kilogram. On the other hand, core loss (iron loss),

$$P_C = P_H + P_E \quad \text{.....3.43}$$

Hysteresis core loss *PH*, W/kg

$$P_H = \frac{2}{3}P_C \text{.....3.44}$$

Eddy current core loss *PE*, W/kg

$$P_E = \frac{1}{3}P_C \text{.....3.45}$$

As illustrated in *Graph 3* (Appendix II), Energy equivalent to the area inside the hysteresis loop is wasted each time the magnetic material is driven around it. As a result, the product of the cycle frequency and the hysteresis loop area determines the hysteresis power loss. An approximate representation of the outer hysteresis loop area w_H , J/m^3, is a rectangle with $2B_s$ for height and $2H_c$ for width.

$$w_H = 2B_s x 2H_c \text{.....3.46}$$

In other term the outer loop hysteresis core loss P_c, W/kg, can be found by the hysteresis loop area divided by the magnetic material density ρ and multiplying it by the cyclic frequency *f* gives as follows.

$$P_H = \frac{4B_S H_C f}{\rho} \text{.....3.47}$$

From the *Table 0.6* (Appendix I) iron loss P_c ($W_{1.5/50}$) corresponding to maximum magnetic induction 1.5T at a frequency of 50Hz is 0.7watt/kg and density ρ of FeSi 3.2 wt% silicon 7500kg/m^3 respectively.

$$P_H = \frac{4x1.5\ Wb/m^2\ x\ 26\,At/m\ 50Hz}{7500kg/m^3}$$

$$P_H = 1.04watt$$

As a result of the above Equation $P_H = \frac{2}{3}P_C$.....3.44 solves for core loss,

$$P_c = \frac{3}{2}P_H = \frac{3}{2}x1.04\ watt$$

$$P_c = 1.56watt$$

From the datasheet, the core loss corresponding to maximum saturation is expressed in terms of power per mass (watt/kg) therefore by multiplying by mass the length of the core magnet can be found.

$$P_C(watt) = P_C\left({}^{watt}/_{kg}\right) x\ M_{core}(kg) \text{.....3.48}$$

Hence mass is the product of volume and density ($V_{vol}x\,\rho$) and volume is an area by length ($A_{core}\,x$ MPL) substitute into mass and solve for magnetic path length (MPL).

$$P_C(watt) = P_C(watt/kg)x\left(A_{core}(m^2)\,xMPL(m)\,x\,\rho(kg/m^3)\right) \text{.....3.49}$$

$$1.625watt = 0.7\,watt/kg\;\; x\; 0.0016m^2\; x\; 7500\,kg/m^3 x\;\; MPL$$

$$\text{MPL} = \frac{1.56watt}{0.7\,watt/kg\;\; x0.0016m^2\; x\; 7500\,kg/m^3}$$

$$\text{MPL} = 0.187m$$

An alternative method for calculating the magnetic path length MPL involves computing the arithmetic mean of the internal and external perimeters. This has a significant impact on small W_{core}. We can calculate the corner reluctance by including the folding effect of the core using straightforward calculations.

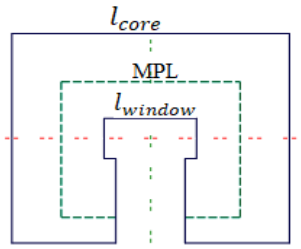

Figure 3.14: Magnetic path length

Therefore, from the relation to the length of the core l_{core} and the width of the window l_{window} from the diagram in Figure 3.1 can be calculated,

$$MPL = 4(l_{core} - 2W_{core} + 0.56W_{core}) \text{.....3.50}$$

$$0.187m = 4(l_{core} - 2x0.030m + 0.56x0.030m)$$

$$l_{core} = 0.09m$$

Similarly, the inner core length (window width),

$$l_{window} = l_{core} - 2W_{core} \text{.....3.51}$$

$$l_{window} = 0.09m - (2x0.030)m$$

$$l_{window} = 0.03m$$

II. Design of Magnetic Circuit

Electromagnetic circuits can be thought of in a similar way to electrical circuits where the magnetomotive force (MMF), flux Φ, and reluctance $\mathcal{R}$ of a magnetic circuit are equivalent to the voltage, current, and resistance respectively. The magnetic circuit is presented in Figure 3.15

according to electrical analogy, a coil with N turns of winding and i amperes (amps) induces a MMF Ni that impulses the Φ through a region with an A_{core} and MPL. In the electrical analogy, a voltage v induces EMF that impulses an electrical current i through area. The amount of MMF needed per unit of Φ is named reluctance. Hence, the system has four regions such as the core magnet with north and south poles, the first air gap, the conducting disk, and the second air gap. Therefore, $\mathcal{R}_{\text{core}}$ stands for the core reluctance, $\mathcal{R}_{\text{airgap1,2}}$is the reluctance of the first and second airgap and $\mathcal{R}_{\text{cond}}$ is the conducting disk reluctance.

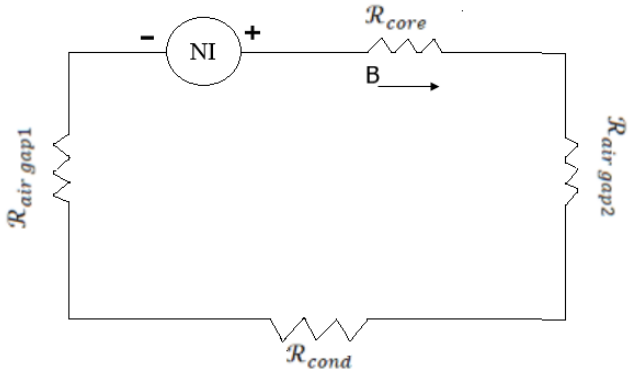

Figure 3.15: Magnetic circuit

From the magnetic Cricut above Figure 3.15 the summation of all reluctance gives us total reluctance on the system,

$$\mathcal{R}_{total}=\mathcal{R}_{core}+\mathcal{R}_{airgap\,1}+\mathcal{R}_{cond}+\mathcal{R}_{airgap2} \quad \text{.....3.52}$$

The reluctance of the magnetic core $\mathcal{R}_{core}$ is the rate of length of the core and the product of permeability of iron silicon steel 3.2 wt% silicon from *Table 0.6* (Appendix I) the relative permeability $\mu_{r\ FeSi}$ are 15,000 and a crossectional area A_{core} of the core is $0.0016m^2$. the reluctance on both airgaps $\mathcal{R}_{airgap1,2}$ is the length of airgap which is considered as 1mm by the permeability of air μ_o $4\pi x10^{-7}$ H/m and the airgap area $A_{airgap1,2}$. the reluctance for the conducting disk is also the rate of the thickness of the disc and the permeability of aluminum $\mu_{r\ Al}$ is a unit and area of the disk exposed to the magnetic field the same as the cross-section of the magnet.

$$\mathcal{R}_{total}=\frac{MPL_{coe}}{\mu_o\mu_{r\ FeSi}A_{core}}+\frac{l_{airgap1}}{\mu_o A_{airgap1}}+\frac{d}{\mu_o\mu_{r\ Al}A_{cond}}+\frac{l_{airgap2}}{\mu_o A_{airgap2}} \quad \text{.....3.53}$$

Hence the area is equal and air permeability μ_o common by rewriting Equation 3.53 as follows

$$\mathcal{R}_{total} = \frac{1}{\mu_o A_{core}}\left(\frac{MPL_{core}}{\mu_{r\ FeSi}} + l_{airgap1} + \frac{d}{\mu_{r\ Al}} + l_{airgap2}\right)$$

$$\mathcal{R}_{total} = \frac{1}{4\pi x 10^{-7}\ \mathrm{H/m}\ x\ 0.0016m^2}\left(\frac{0.187m}{15000} + 0.001m + \frac{0.0205}{1} + 0.001m\right)$$

$$\mathcal{R}_{total} = 11.2x\ 10^6 H^{-1}$$

When all systems follow the conservation of energy principle found in the first rule of thermodynamics, there is an energy balance. Energy is therefore neither created nor destroyed. For a general system, an energy balance may thus be expressed as follows: the change in mechanical energy ΔU_m plus the change in electric energy input ΔU_e equals the change in energy stored in the system by the magnetic field ΔU_f. The equation that follows shows how this energy balance is represented.

$$\Delta U_e = \Delta U_f + \Delta U_m \quad \text{.....3.54}$$

By integrating the coil voltage and current over time, one can determine the input electrical energy as follows.

$$U_e = \int_0^t vi\ dt = vit \quad \text{.....3.55}$$

Where v is the voltage of a battery which is $12v$ volt, i stands for the current induced by the electromagnet and t is the time used to stop the car.

By integrating it over the magnetization curve, the stored magnetic field energy is determined. Examining the region of integration, which is located above the magnetization curve, or computing it The permeability μ or inductance L of linear materials is always the same. Since there is no magnetic flux when there is no current, there is no stored energy. When resistive losses are taken into account, the energy stored by a current-carrying inductance is equal to the effort needed to create the magnetic field and current flow through the inductance from zero. Consequently, for a given current, inductance is also proportional to the energy stored in the magnetic field. As long as there is a continuous current, this energy is stored. A drop in current results in a corresponding decrease in the magnetic field, which causes a voltage to be induced in the conductor in the opposite direction—positive at the end where the current exits and negative at the entry point. In the external circuit, this releases magnetic energy that has been accumulated.

$$U_f = \int_0^t Li\ di = \frac{1}{2}Li \quad \text{.....3.56}$$

The product of the mechanical force F that results in KE and the distance along longitudinal x is equal to the change in mechanical energy ΔU_m

$$U_m = U_{translation} + U_{rotational} = \frac{1}{2}m_t {V_x}^2 + \frac{1}{2}I{\omega_w}^2 \quad \text{.....3.57}$$

Where m_t is the vehicle quarter mass carried by wheel V_x a maximum speed of the vehicle, I and ω_w are inertia and angular speed of the wheel.

Consider the input energy or the electrical energy U_e at no load condition which is zero, to calculate the unknown value of inductance L,

$$\frac{1}{2}Li^2 = \frac{1}{2}m_t {v_x}^2 + \frac{1}{2}I{\omega_w}^2 \quad \text{.....3.58}$$

Solve for inductance L,

$$L = \frac{m_t {v_x}^2 + I{\omega_w}^2}{i^2} \quad \text{.....3.59}$$

Hence energy is a product of power and time, Current can be calculated from the relation of energy and power P.

$$U = Pt = vit \quad \text{..... 3.60}$$

Power is a measure of the rate of change of energy in a system. therefore, the power dissipated by the braking is assumed by the negative derivative of the vehicle's kinetic energy by time.

$$P = -\frac{dU}{dt} \quad \text{..... 3.61}$$

From Equation 3.57 The kinetic energy is,

$$P = -\frac{dU}{dt} = -\frac{d}{dt}\left(\frac{1}{2}m_t {v_x}^2 + \frac{1}{2}I{\omega_w}^2\right) \quad \text{..... 3.62}$$

Mass and moment of inertia are constants, besides from chain's rule $\frac{d}{dt}({v_x}^2) = 2v_x\frac{dv_x}{dt}$ therefore, Equation 3.62 is simplified as,

$$P = -\frac{dU}{dt} = -\left(m_t v_x \frac{dv_x}{dt} + I\omega_w \frac{d\omega_w}{dt}\right) \quad \text{.....3.63}$$

Where $\frac{dv_x}{dt}$ and $\frac{d\omega_w}{dt}$ are linear and angular accelerations for braking both negative. Since from the mechanical modeling the linear ($\dot{V}_x$) and angular (α_w) accelerations are found as -19 m/s^2 and -154 rad/s^2 respectively.

$$P = -\left(387.25kg\ x\ 47.2m/s\ x(-19\ m/s^2) + 1.35kg.m^2 x\ 382\ rad/s\ x\ (-154\ rad/s^2)\right)$$

$$P = 426703.6W \approx 426.71\ \text{KW}$$

Therefore, the current from the energy relation equation 3.60 with the source battery voltage 12v is,

$$P = vi$$

$$i = \frac{P}{v} = \frac{426.71\ \text{KW}}{12v} = 35558.64A \approx 35.56KA$$

Consequently, the current is found as $35.56KA$ as well the mass and inertia of the vehicle on the wheel are 387.25kg and 1.35kgm^2 respectively and the vehicle speed is 47.25m/s. As a result, by substituting the above parameters into Equation 3.59 inductance is,

$$L = \frac{387.25kg\ x\ (47.2\,m/s)^2 + 1.35\,kg/m^2\ x(382\,rad/s)^2}{(35.56KA)^2}$$

$$L = 8.38\ x\ 10^{-4}\text{H}$$

III. Design of Magnetic Coil

An electromagnetic coil is a wire that functions as an electrical conductor and is shaped like a coil, spiral, or helix. Electric motors, generators, inductors, electromagnets, transformers, and sensor coils devices where electric currents and magnetic fields interface are examples of devices that use electromagnetic coils. A magnetic field is created in the coil by passing an electric current through its wire, or a conductor's emf (voltage) can be produced by an external, time-varying magnetic field passing through the inside coil.

Ampere's rule states that any conductor that has current flowing through it creates a magnetic field that circles the conductor. One benefit of the coil form is that it may produce a magnetic field with a higher intensity for a given current. The magnetic fields generated by each of the N individual turns of wire pass into the coil's core, where they combine (superpose) to create a powerful field. There are more turns of wire since the field generated is stronger. A conductor like a wire experiences an induction of voltage when the external magnetic flux changes, as per Faraday's law of induction. Winding the wire into a coil can increase the induced voltage since the field lines cross the circuit multiple times.

The hollow space in the middle of the coil is known as the core area or magnetic axis. The wire or conductor that makes up the coil is known as the winding, as shown in Figure 3.16. Every wire loop is referred to as a turn N.

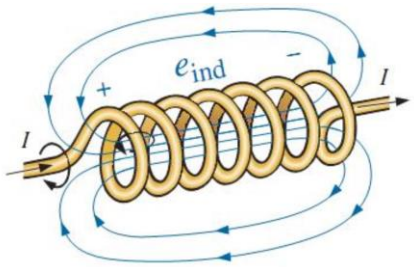

Figure 3.16: Demonstrating the effect of Lenz's law

When a winding is connected to the magnetic core, the electrical-to-magnetic coupling is governed by Ampere's and Faraday's laws. According to the Faraday state, the voltage-induced E across a wire coil is equal to the spiral's number of turns (N) times the magnetic flux change rate (Φ). A magnetic field is created around a conductor as current passes through it, according to ampere as well.

Faraday's law is expressed in equation form as

$$\frac{d\Phi}{dt} = -\frac{E}{N} \quad \text{.....3.64}$$

According to Lenz's law, the induced voltage is pointing in the opposite direction as the change in current that caused it, as indicated by the equation's negative sign.

$$\Phi = \frac{1}{N}\int E\, dt \quad \text{.....3.65}$$

Ampere's law

$$Ni = \int H\, dl = Hl \quad \text{.....3.66}$$

These laws function in both directions. Faraday's law states that the voltage applied to the winding (or the voltage induced in the winding is proportional to dΦ/dt) governs the change in flux Φ. As a result, electrical energy is converted into energy that is either lost or stored in the magnetic system (or electrical energy is converted into stored magnetic energy). The axes may be converted back into the corresponding electrical characteristic of the magnetic core wound with a given number of turns, N, by using Faraday's and Ampere's laws.

$$\Delta U = \int Ei\, dt \quad \text{.....3.67}$$

Where inductance L is derived from the induced voltage and change in current

$$E = L\frac{di}{dt} = N\frac{d\Phi}{dt} \quad \text{3.68}$$

Combined and simplify,

$$L = N\frac{d\Phi}{di} \quad \text{3.69}$$

Where the Φ is a product of B and area

$$L = N\frac{dBA}{di} \quad \text{3.70}$$

Where magnetic flux density is $B = \mu H$ and the field strength from Ampere's law $H = \frac{Ni}{L}$ substitute into the equation

$$L = N\frac{d\ \mu NiA}{di\ l} \quad \text{3.71}$$

Simplify current i from the nominator and the denominator and rearrange the equation

$$dL = d\mu\frac{A}{l}N^2 \quad \text{3.72}$$

Integrate both sides,

$$\int dL = \int d\mu\frac{A}{l}N^2 \quad \text{3.73}$$

therefore, inductance L is

$$L = \mu\frac{A}{l}N^2 \quad \text{3.74}$$

Hence the reluctance $\mathcal{R}$is,

$$\mathcal{R} = \frac{l}{\mu A} \quad \text{3.75}$$

substitute Equation 3.75 into 3.74

$$L = \frac{N^2}{\mathcal{R}} \quad \text{3.76}$$

The typical criteria in coil design are to calculate the number of turns N, mean turn length, the wire size/diameter/ AWG, the temperature change Δt, the resistance of coil R, and the inductance L, given the required amp-turns Ni.

The number of turns N can be calculated from equation 3.76,

$$N^2 = L\ x\mathcal{R} \quad \text{3.77}$$

$$N^2 = 8.38\ x\ 10^{-4}\text{H}\ x\ 11.2\ x\ 10^{6}H^{-1}$$

$$N = \sqrt{8.38\ x\ 10^{-4}\text{H}\ x\ 11.2\ x\ 10^{6}H^{-1}}$$

$$N = 96.8\, turns = 97 turns$$

The mean turn length can be determined from the inductance formula which is inversely proportional to each.

$$L = N^2 \frac{\mu_0 A_{core}}{l_{coil}} \quad \text{.....3.78}$$

Where the area of the core A_{core} and permeability of the air μ_0 are $0.0016m^2$ and $4\pi\ x\ 10^{-7}$ H/m respectively.

$$l_{coil} = N^2 \frac{\mu_0 A_{core}}{L}$$

$$l_{col} = \frac{4\pi\ x\ 10^{-7}\text{H/m}\ x\ 0.0016m^2\ x\ 97^2}{8.38\ x10^{-4}H}$$

$$l_{coil} = 0.0226m$$

3.3.2.3 Thermal Analytical Model of Brake

During the retardation of the car, the KE of the car is transformed to thermal energy, resulting in intense heating of the braking disks of the car. If the disks overheat, the electromagnet device (core and wire) deterioration brake performance or may stop working in the worst-case melt. On that account, it's important to consider the maximum surface temperature during the design process. For design optimization, material specification, and brake performance prediction brake thermal analysis is also crucial.

The temperature change is linearly dependent on heat dissipated from the system. For that reason, the heat transfer between the brake and surroundings is due to only convection and can be expressed as,

$$Q = hA\Delta T \quad \text{..... 3.79}$$

where Q is the heat transferred per unit time which is equal to the power dissipated 426.71 KW from Equation 3.64, A the area available for the flow of heat, ΔT the temperature difference, and h is known as the overall heat transfer coefficient for aluminum is 22.2 KW/m^2 K.

$$Q = h\ x\ (\pi {R_w}^2)\ x\ \Delta T$$

$$426.71\ x\ 10^3\text{W} = 22.2\ x\ 10^3\ \text{W}/m^2K\ x\ \pi\ (0.1235^2 - (0.1235 - 0.05)^2)\ m^2\ x\ \Delta T$$

$$\Delta T = 621.137K$$

Therefore, the maximum temperature is,

$$\Delta T = T_{max} - T_a$$

$$T_{max} = \Delta T + T_a = 621.137K + 293.15K$$

$$T_{max} = 914.287\ K$$

Based on the maximum temperature the resistance of the wire which helps to determine the size of the wire is gained by execution of energy balance at the surface of the brake of thermal energy and electrical energy. It's important to consider some Constant properties such as the heat transferring between the brake and surroundings being by only convection and radiation, Steady-state 1D heat transfer through each surface of the brake, and the radiation transfer between the skin surface and the surroundings being among a minor surface and a huge enclosure at the ambient temperature.

$$Q - U_e = 0 \quad \ldots\ldots 3.80$$

Where, U_e is electric energy created by ohmic heating by the winding's resistance and Q is the thermal energy discharge via convection and radiation from the surface.

The electrical energy due to ohmic relation is,

$$U_e = i^2R = \frac{v^2}{R} \quad \ldots\ldots 3.81$$

the voltage v is applied at the of windings 12volt and R is the resistance of the wire,

The heat transfer from convection and radiation is,

$$Q = Q_{convection} + Q_{radation} \quad \ldots\ldots 3.82$$

$$Q = hA(T_{max} - T_a) + \varepsilon\sigma A({T_{max}}^4 - {T_a}^4) \quad \ldots\ldots 3.83$$

To solve for the resistance of the winding by replacing Equations 3.81 and 3.83 by rewriting Equation 3.80 as below, where h is the coefficient of convection heat transfer, ε is emissivity of the surface constant σ is Stefan-Boltzmann constant, 5.67x10^{-8}

$$hA_{winding}(T_{max} - T_a) + \varepsilon\sigma A_{winding}({T_{max}}^4 - {T_a}^4) = \frac{V^2}{R}$$

$$0.05m\ x\ 0.0228m[\ 22.2x10^3\ W/m^2K\ x(621.137K)$$

$$+\ 0.09x\ 5.67\ x\ 10^{-8}\ W/m^2K^4\ ((914.287K)^4 - (293.15K)^4)] = \frac{(12vol)^2}{R}$$

$$R = 0.0092\ \Omega$$

Consequently, the wire diameter can be determined from the resistivity of the material, the resistivity of aluminum-silicon wt 1% silicon is $2.7\ x\ 10^{-8}\Omega$m.

$$R = \frac{\rho l_{wire}}{a_{wire}} = 4\frac{\rho l_{wire}}{\pi {d_{wire}}^2}$$

Rearranging equation,

$$d_{wire} = \sqrt{4\frac{\rho l_{wire}}{\pi R}}$$

$$d_{wire} = \sqrt{\frac{4\ x\ 2.7\ x\ 10^{-8}\Omega m\ x\ 0.0226m}{\pi\ x\ 0.0092\ \Omega}}$$

$$d_{wire} = 3\ x\ 10^{-4}m$$

The number of turns and dimensional parameters of electromagnetic wire is found in the design as $97turns$ with 0.0226m coil length and $3\ x\ 10^{-4}m$ diameter of the wire. The output geometrical configuration is illustrated in *Figure 3.17*.

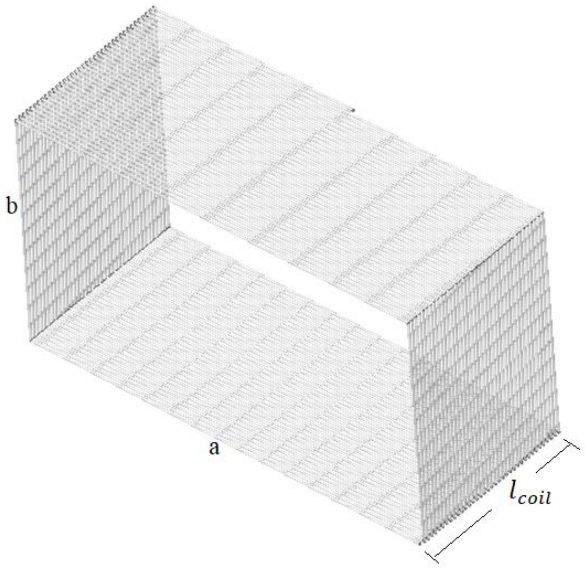

Figure 3.17: Rectangular winding

3.4. Simulation and Design Optimization

Simulation and optimization processes are carried out using ANSYS a Finite Element Analysis FEA software that is applicable to simulate models on a computer of machine parts, structures, and electronics, or applicable for analyzing the structural property, thermal distribution, electromagnetism, fluid flow, and extra characteristics. In this research work, ANSYS workbench 2020 R2 is used to analyze the electromagnetic brake system.

I. Geometric modeling of electromagnetic brake system

In this thesis work, the geometry is developed using ANSYS SpaceClaim 2020 R2 which is a unique user interface and multipurpose toolset modeling technology that aids in generating and altering imported geometry without the difficulty related to old CAD systems. SpaceClaim offers experts with tools for stepping up geometry preparation for simulation. By dealing with the geometry, analysts can vest simulation-driven design, end delays, and without difficulty understanding how design changes influence outcomes. The electromagnetic braking system is composed of three major components represented below in Figure 3.18, a rotating disk, a magnetic coil wound around the magnetic core that acts as an actuator, and an air enclosure which is important in the analysis of magnetostatics analysis.

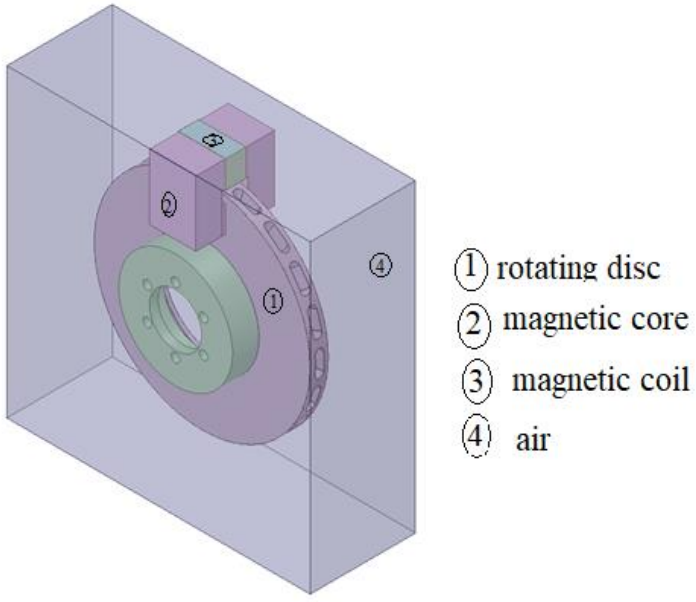

Figure 3.18: 3D modeling electromagnetic brake system ANSYS SpaceClaim

II. Finite element analysis using ANSYS workbench 2020 R2

The performance of the electromagnetic brake can be estimated accurately at the design stage using the finite element method FEM, because it approximated nonlinear magnetic material properties it is best to perform simulation electromagnetic field analysis.

The finite element FE method has revealed its reliability in the study of contactless magnetic braking than analytical modeling which uses many assumptions that may decrease the accuracy of the result. It provides a complete solution for electromagnetic brakes considering most real-life conditions. ANSYS workbench 2020 R2 is a 3D FEM simulation software, which is implemented to analyze the electromagnetic, thermal, and structural behavior of the electromagnetic braking system under steady-state conditions.

3.4.1. Magnetostatic Analysis

Static magnetic field analysis is known as magnetostatics. Here the currents are DC, or steady current, as opposed to the stationary charges in electrostatics. Ironically, as long as the currents do not alternate quickly, magnetostatics remains a reliable approximation even in non-static situations. In addition, the null hypothesis states that Maxwell's displacement current, which relates the electric and magnetic fields, exists.

This analysis applies only to 3-D geometry. Conductor bodies are defined from solid CAD geometry from SpaceClaim. the physical geometry is surrounded by air to simulate the magnetic field it needs to be modeled as part of the total geometry represented in Figure 3.18 the electromagnetic braking system is enclosed. The resulting model has to be a single multi-body part that contains the physical braking system geometry and the air.

To carry out the simulation Parts must be linked with materials. Material properties can be isotropic or orthotropic, constant or temperature-dependent, linear (such as in linear elastic analysis), or nonlinear (such as in damage mechanics analysis). One of the most crucial elements of a good analysis is inserting the correct properties of the material.

Defining the properties of magnetostatics material in a magnetostatics simulation starts by clicking on the pull-down menu under type to define the material parameters and to determine the magnetic properties of the material value by selecting relative permeability μ is which is $\mu_0 * \mu_r$ relative permeability μ_r multiplied by the magnetic coercivity. Relative permeability is either a simple

linear μ_r or nonlinear BH curve or/and anisotropic bulk conductivity needs to determine the current-carrying conductor's distribution of current but has no effect on the magnetic analysis parts which is simple or anisotropic magnetic coercivity applied to describe magnetic material's permanent magnetization.

The magnetic field simulation supports the following four material properties classes:

The first one is called Linear soft magnetic materials and is applicable for low-saturation cases. It must have relative permeability. This could be orthotropic or constant concerning the body's coordinate system. Laminate materials are frequently simulated using orthotropic characteristics.

The second is Linear hard magnetic materials which apply to model permanent magnets. coercive force and residual induction are needed and the magnet's demagnetization curve is assumed to be linear.

Third is Nonlinear soft magnetic material the material that is applied for model devices that undergo magnetic saturation. A B-H curve is obligatory. In any of the orthotropic directions BH curve is assigned for orthotropic materials, while in other directions selecting a relative permeability is constant.

At last Nonlinear hard magnetic material, is the material applied to model nonlinear permanent magnets. the demagnetization curve for the material is gained from A B-H curve modeling.

The materials selected for the system are liner soft magnetic material available in the software as shown in Figure 3.19 and some properties are inserted from standard materials properties.

Outline of Schematic A2, B2, C2, D2: Engineering Data

	A	B	C	D	E
1	Contents of Engineering Data			Source	Description
2	Material				
3	Air			Fluid_Materials.xml	
4	Air 2			General_Materials.xml	General properties for air.
5	Aluminum Alloy			General_Materials.xml	General aluminum alloy. Fatigue properties come from MIL-HDBK-5H, page 3-277.
6	Aluminum silicon 1 % si			General_Materials.xml	General aluminum alloy. Fatigue properties come from MIL-HDBK-5H, page 3-277.
7	iron silicon 3.2 % si			Magnetic_B-H_curves_Soft_Materials.xml	
*	Click here to add a new material				

Properties of Outline Row 7: iron silicon 3.2 % si

	A	B	C	D	E
1	Property	Value	Unit		
2	Material Field Variables	Table			
3	Density	7500	kg m^-3		
4	Isotropic Secant Coefficient of Thermal Expansion				
5	Coefficient of Thermal Expansion	1.47E-05	C^-1		
6	Isotropic Elasticity				
7	Derive from	Young's Modulus and P...			
8	Young's Modulus	2.07E+11	Pa		
9	Poisson's Ratio	0.3001			
10	Bulk Modulus	1.7259E+11	Pa		
11	Shear Modulus	7.9609E+10	Pa		
12	Tensile Yield Strength	393	MPa		
13	Tensile Ultimate Strength	531	MPa		
14	Isotropic Thermal Conductivity	73	W m^-1 C^-1		
15	Specific Heat, C_p	460.5	J kg^-1 C^-1		
16	Isotropic Relative Permeability	15000			
17	Isotropic Resistivity	4.8E-07	ohm m		

Figure 3.19: Linear "soft" magnetic materials properties

By describing every node, its location, and the connectivity between each element, the model geometry may be found. The program can combine the element equivalent force vector and the element stiffness matrix to derive the global equilibrium equations thanks to the connectivity information. An analysis based on magnetostatics does not support connections. The precision of the solution depends on the mesh density. In order to calculate force or torque accurately, the air areas around the objects of interest must have a fine mesh. It is recommended to minimize the use of pyramid elements in key zones as represented in Figure 3.20.

Details of "Mesh"

Display	
Display Style	Use Geometry Setting
Defaults	
Physics Preference	Electromagnetics
Element Order	Quadratic
Element Size	18.0 mm
Sizing	
Use Adaptive Sizi...	Yes
Resolution	Default (4)
Mesh Defeaturing	Yes
Defeature Size	Default
Transition	Fast
Span Angle Center	Coarse
Initial Size Seed	Assembly
Bounding Box Di...	505.31 mm
Average Surface ...	3619.7 mm²
Minimum Edge L...	4.4131e-002 mm
Quality	
Inflation	
Advanced	
Statistics	
Nodes	34115
Elements	24117

Figure 3.20:Meshing details

Accordingly, the meshing selected for the system is default meshing with element size 18mm with total elements 24117 and 34115 nodes as shown in above Figure 3.20. but the student version ANSYS Inc only can support less than 32000 nodes by adjusting the nodal size by default Figure 3.21, the program will utilize the direct solver. Convergence is assured by the direct solver.

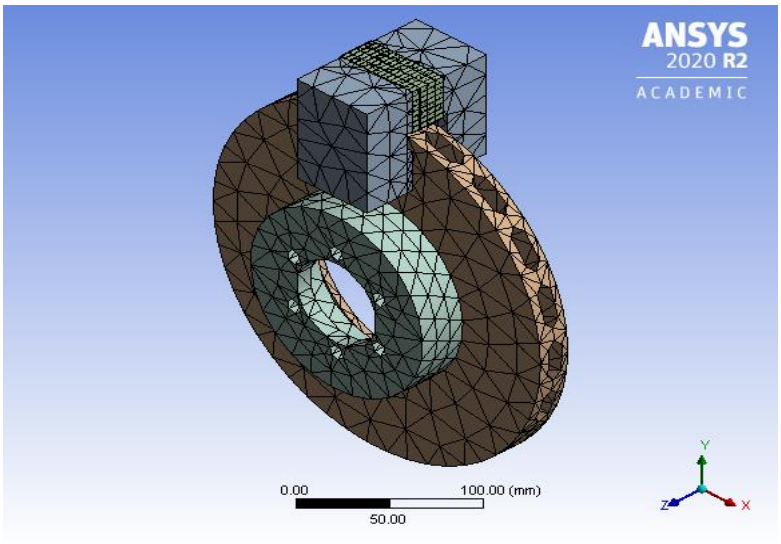

Figure 3.21: Meshed 3D model for magnetostatic analysis

general control over the solution process is offered by the Analysis Settings details. adjust the number of steps in the analysis and an end time for each step hence manual and auto-time stepping controls can be specified. in static analyses tracking mechanism is a Time. so, the analysis setting is controlled in seven steps and the ending time is specified as 2.5 seconds.

A constraint on the field domain is regarded as a boundary condition. A boundary condition that is not zero and results in an electric or magnetic excitement of the system is called an excitation. The field domain at its exterior faces is subject to boundary conditions. Magnetic flux is applied parallel to the air cage, and conductors are excited as shown in Figure 3.22.

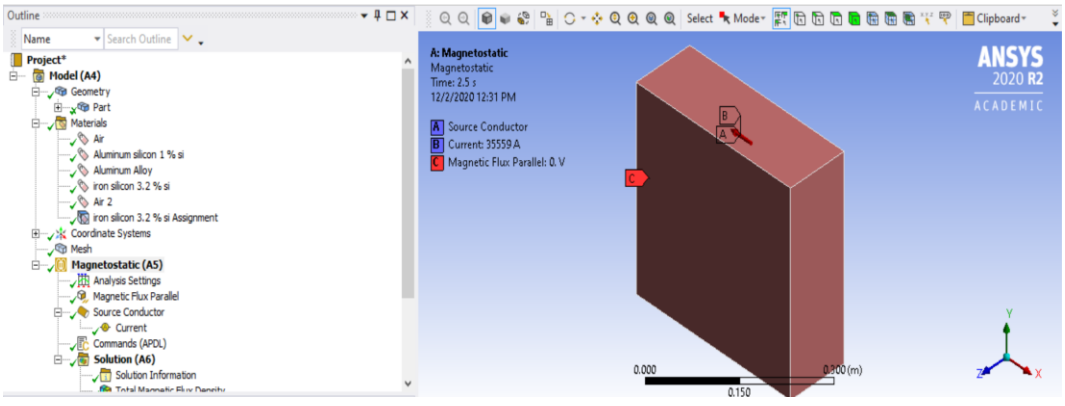

(a)

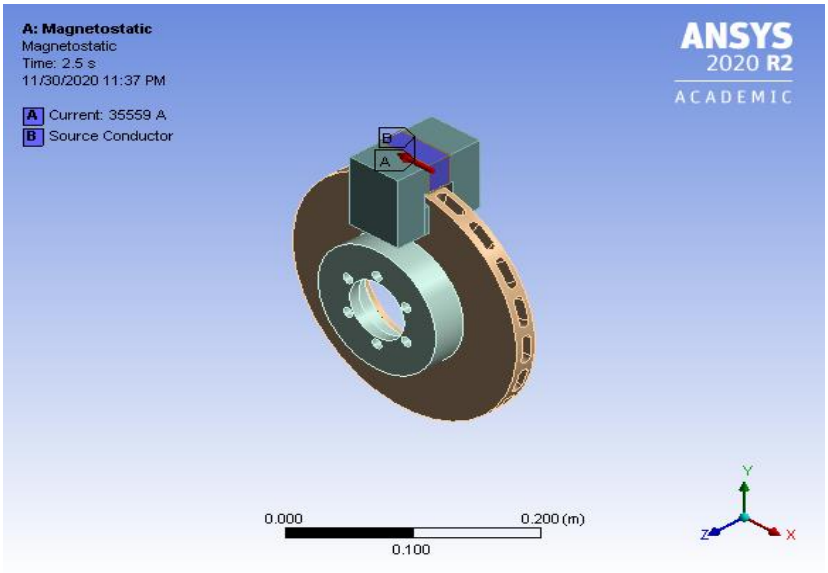

b)

Figure 3.22: boundary and Loading conditions a) magnetic flux, source conductor, and applied current b) source conductor and applied current

The solver's listing output is continuously updated by the solution output, which also offers insightful details on how the structure behaved during the analysis. This printout's convergence data output can be graphically shown, as detailed in the section on solution information. For analyses including magnetostatics, adaptive mesh refinement is possible.

A magnetostatic analysis provides a result in several items, as shown in Figure 3.23

- Flux Density
- Directional Flux Density
- Field Intensity
- Directional Field Intensity
- Force
- Directional Force/Torque
- Energy probe (magnetic co-energy)
- Flux Linkage
- Error (Magnetic)

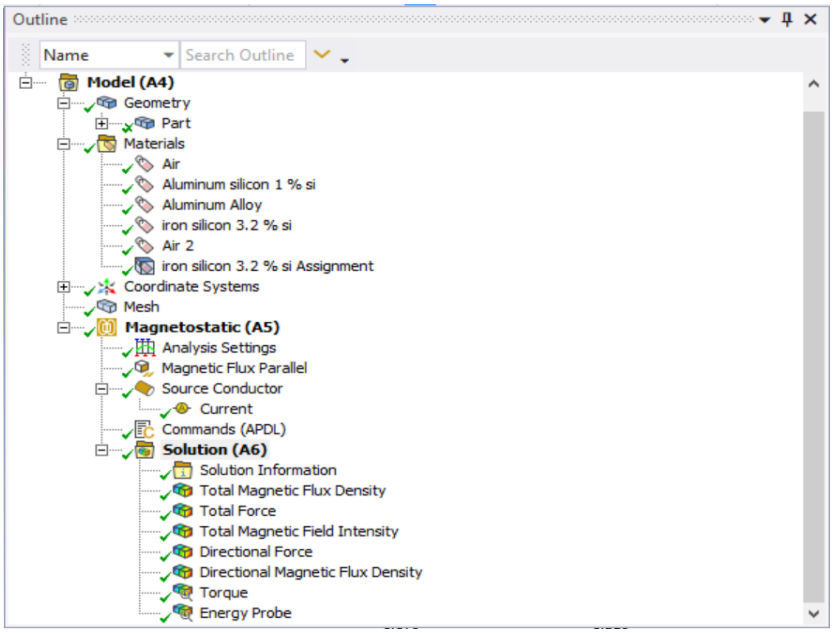

Figure 3.23: Solver details in ANSYS Mechanical

3.4.2. Optimization

To improve the performance of the electromagnetic braking is Optimized through the simulation. The theoretical foundations of electromagnetic field analysis are presented first. then a demonstration of the finite element model's assumptions and simulation outcomes. At the cost of little input power, an efficient electromagnetic brake can provide a significant magnetic force that can produce a significant braking torque. A quicker response is also preferable, especially for situations where delays negatively impact task efficiency. The fact that the more coil current there is for a given brake volume, the more magnetic force it produces, but it also consumes more power, was realized by the development of analytical models. As an alternative, increasing the coil's turns can reduce the input power but also raise the inductance. The braking response is therefore diminished. Brief background knowledge regarding optimization techniques, in general, would be helpful to comprehend the method selection process before discussing the approaches used to solve the electromagnetic braking system optimization challenge.

The most crucial variables for the brake performance in FEA are the air gap length and the coil's ampere-turn count. For this reason, parametrical simulations are used in the FEA. The coil number of turns and appropriate conductor radius as shown by the flow chart in Figure 3.24 are where optimization begins. To compute conductor radius with varying numbers of turns, a method is devised.

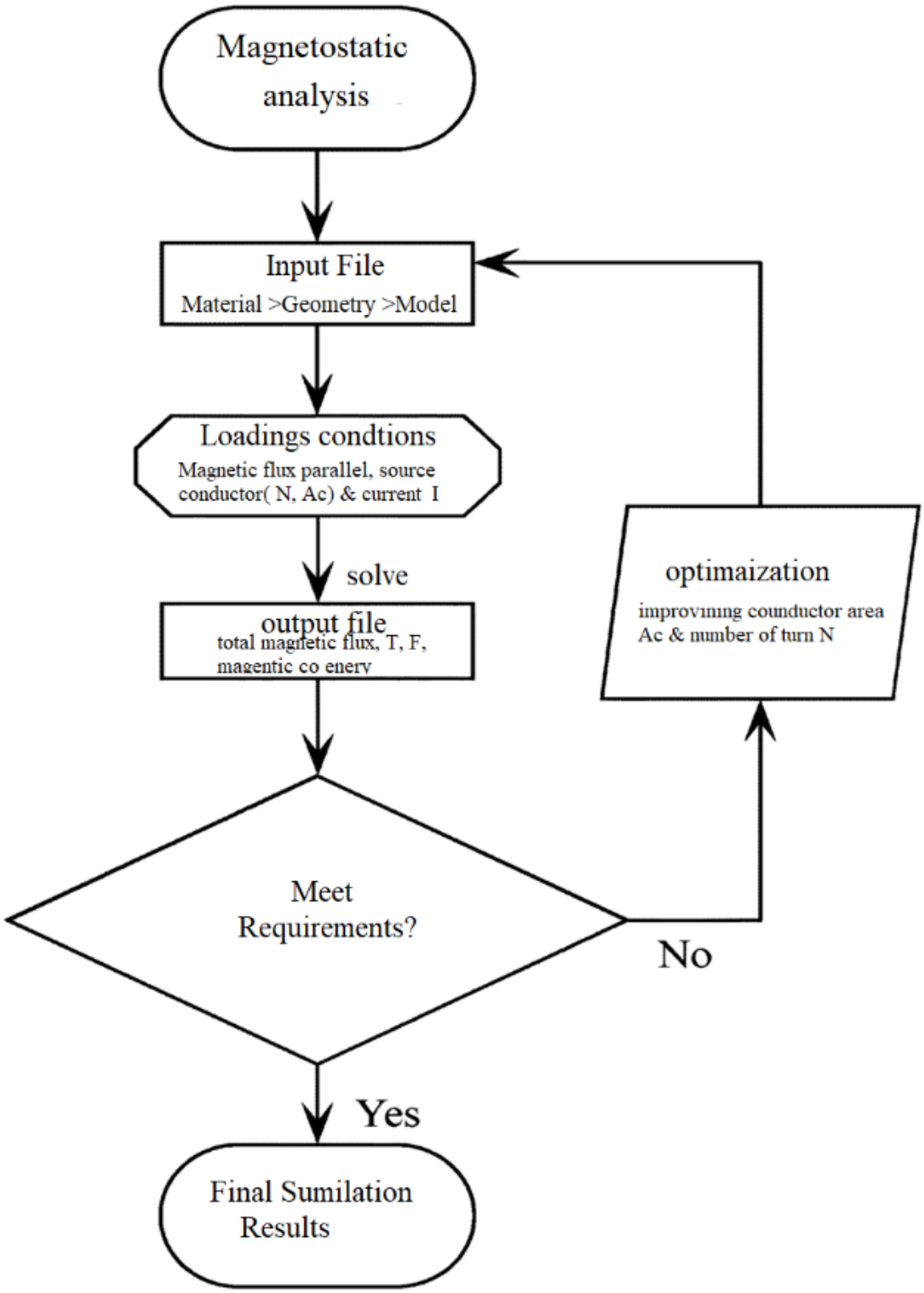

Figure 3.24: Optimization flow chart

3.4.3. Steady-State Thermal Analysis

The general topic of thermal analysis is heat transmission in solid materials. Energy is transferred in a solid body from a high-temperature area to a low-temperature area. The material thermal conductivity, cross-sectional area, and temperature gradient in the normal direction all affect the rate of heat transfer per unit area, which is inversely proportional to distance. The terms transient and steady-state thermal analysis are used to describe the thermal analysis. As a result, if heat flow remains constant, the issue is one of steady-state analysis rather than static heat flow. A problem is considered transitory if the amount of heat flow varies over time.

the thermal response to heat loads is calculated by steady-state thermal analyses depending on the given temperatures applied to convection conditions or both. boundary conditions and all thermal loads assumed in analyses of steady-state thermal. changes over time are not evaluated under this form of analysis.

The characteristics of steady-state thermal analysis for models are stated as follows

- temperature-dependent thermal conductivity
- temperature-dependent convection coefficients
- radiation conditions

Either linear, with constant material characteristics, or nonlinear, with temperature-dependent material properties, can be found in a steady-state thermal analysis. Most materials' thermal characteristics, as seen in Figure 3.25 do change with temperature; however, the analysis is typically nonlinear. The analysis becomes nonlinear when radiation effects are considered. Thermal conductivity is the sole material attribute needed for a steady state.

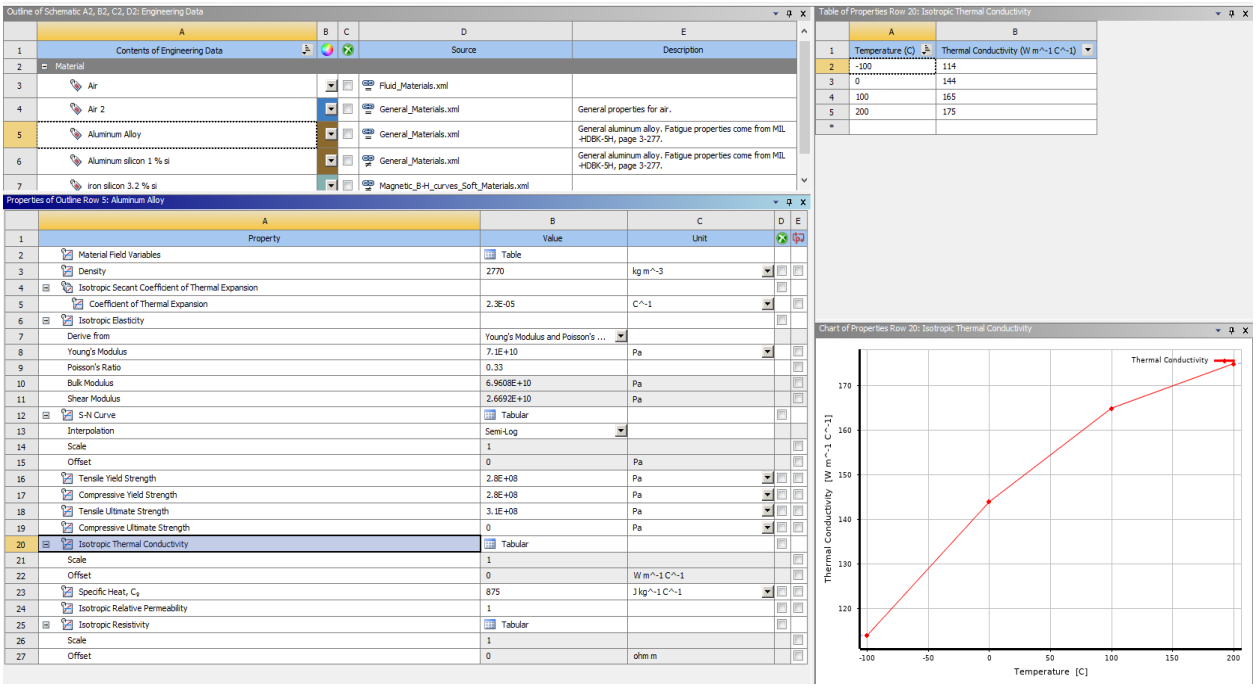

Figure 3.25: Thermal Materials Properties

The other important parameter in steady-state thermal analysis is the thermal contact between bodies. In assemblies, contact zones are automatically formed to facilitate heat transfer between components, just like in structural analyses. Contact zones between the solid bodies are automatically formed when importing assemblies of solid parts. Contact between surfaces permits non-matching meshes at the edges of solid components. Heat transfer between components in an assembly is enabled by contact.

There are many different contact behaviors in simulation; the contact type is intended for structural applications. Heat transfer will happen if the pieces are first in contact with one another. Heat will not be transferred between the parts if they are initially not in contact.

In this case, as shown in Figure 3.26 and Figure 3.27, the contact between the braking actuator which is the electromagnetic device, and the rotating disk is frictionless contact that exists a gap between them. To account for any little gaps in the model, the pinball region is automatically defined and assigned to a reasonably small number. Therefore, a 1 mm radius pinball is used.

Details of "Frictionless - Multiple To Multiple"

Scope	
Scoping Method	Geometry Selection
Contact	1 Face
Target	1 Face
Contact Bodies	Multiple
Target Bodies	Multiple
Protected	No
Definition	
Type	Frictionless
Scope Mode	Manual
Behavior	Program Controlled
Trim Contact	Program Controlled
Suppressed	No
Advanced	
Formulation	Program Controlled
Small Sliding	Program Controlled
Detection Method	Program Controlled
Penetration Tolerance	Program Controlled
Normal Stiffness	Program Controlled
Update Stiffness	Program Controlled
Stabilization Damping Factor	0.
Thermal Conductance	Program Controlled
Pinball Region	Radius
Pinball Radius	1.e-003 m
Time Step Controls	None
Geometric Modification	

Figure 3.26: Manual contact region details

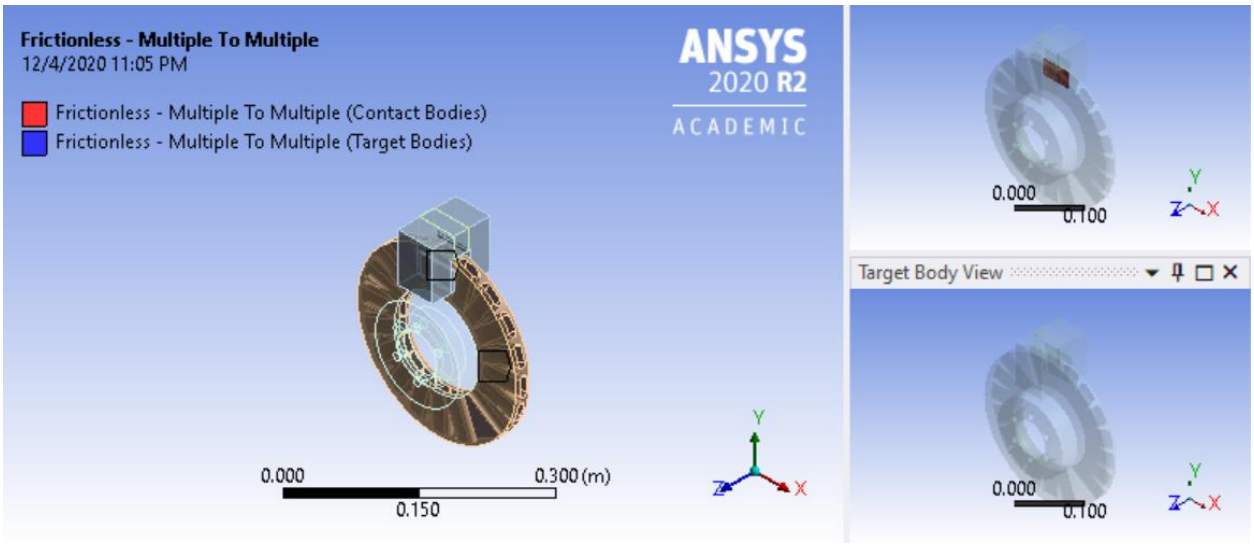

Figure 3.27: 3D views of the contact body

Meshing in thermal analysis is a similar procedure as magnetostatic analysis except changing the physical preference into mechanical this meshing shown in Figure 3.28, is common in the next

analysis static structural analysis. The meshing is corrected to be suitable for processing the analysis with 28340 nodes and 13006 elements.

Details of "Mesh"

Display	
Display Style	Use Geometry Setting
Defaults	
Physics Preference	Mechanical
Element Order	Program Controlled
Element Size	Default
Sizing	
Quality	
Check Mesh Qua...	Yes, Errors
Error Limits	Aggressive Mechanical
Target Quality	Default (0.050000)
Smoothing	Medium
Mesh Metric	None
Inflation	
Advanced	
Number of CPUs ...	Program Controlled
Straight Sided El...	No
Rigid Body Behav...	Dimensionally Reduced
Triangle Surface ...	Program Controlled
Topology Checki...	Yes
Pinch Tolerance	Please Define
Generate Pinch o...	No
Statistics	
Nodes	28340
Elements	13006

Figure 3.28: Meshing detail for mechanical preference type (thermal and structural analysis)

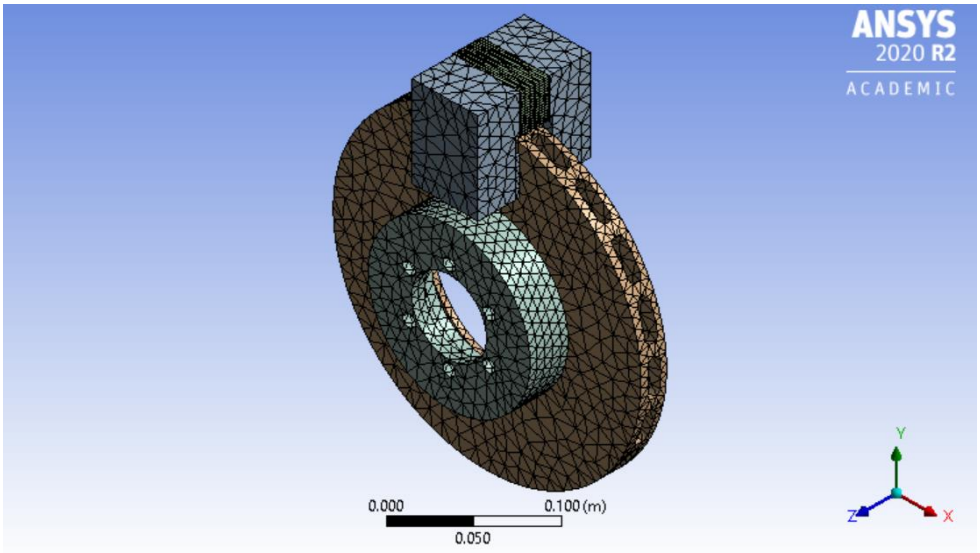

Figure 3.29: A 3D meshed model for mechanical analysis

In the electromagnetic braking system heat is generated through the electromagnetism process and Convection and radiation of heat energy at high temperatures provide the electromagnetic brakes with thermal stability. Therefore, as shown in Figure 3.30 the loading conditions of the system apply

the convection and radiation coefficients of the rotating disk material are important parameters, and the input values of heat energy (heat flow) are derived by magnetic co-energy from the optimized magnetostatic analysis.

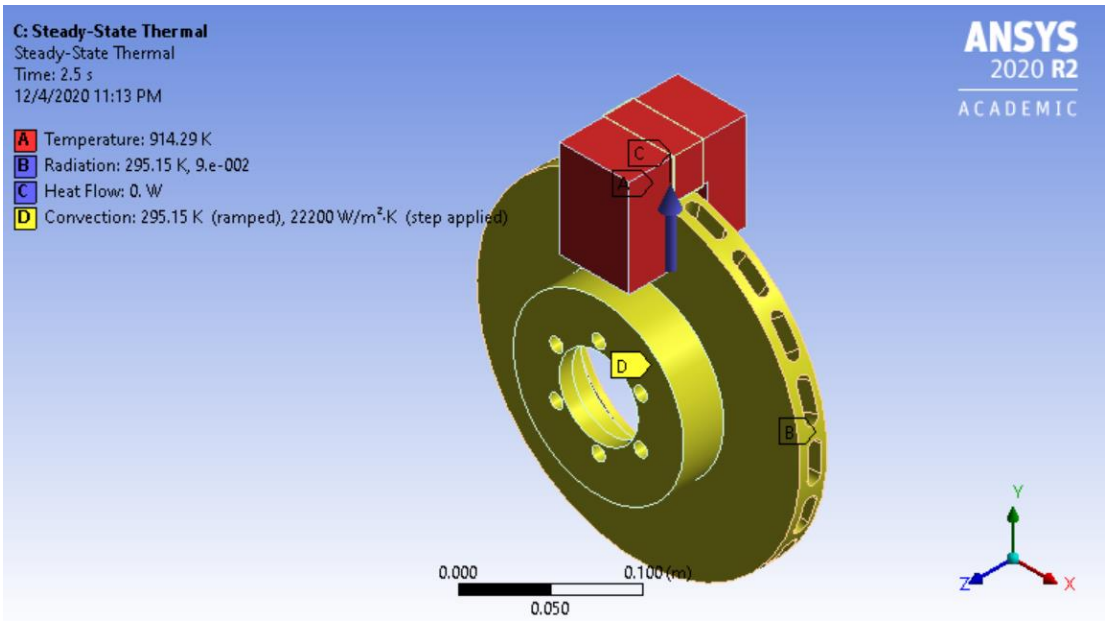

Figure 3.30: Boundary and loading conditions of thermal steady-state analysis

Temperatures in the entire model are calculated using steady-state thermal analysis by interpolating the temperatures measured at the nodes over the elements. To find the temperature gradients, temperatures are then discriminated. Lastly, using the material's thermal conductivity and temperature gradient, the software determines the amount of heat flux. As a result, an analogy where heat flows continuously is provided by a steady-state thermal analysis. It's in equilibrium as well.

Different postprocessing results are available:

- Temperature
- Heat Flux
- "Reaction" Heat Flow Rate

3.4.4. Static Structural

Because structural and thermal analyses are closely analogous, as shown in Figure 3.31, structural analysis can be simply transferred from thermal analysis. In structural analysis, temperature is comparable to displacement, strain to temperature gradient, and stress to heat flow.

Link a structural analysis to the thermal model at the solution level in order to carry out a thermal-stress solution. Any applied structural loads and supports are inserted, together with an imported load branch, into the Static Structural branch.

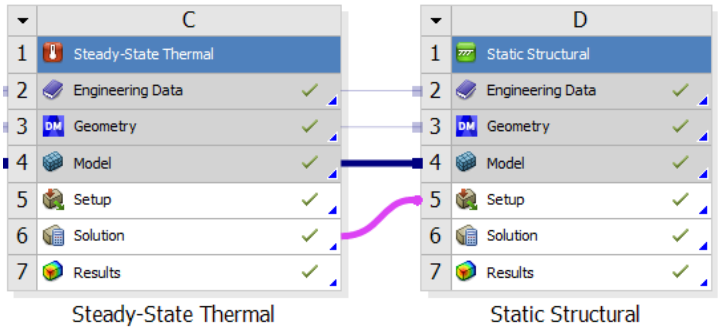

Figure 3.31: Branch analysis element

Material assignment, geometry, and model are imported from the thermal steady-state analysis but the loading and boundary condition are in terms of the 3D shown in Figure 3.32 available for the elements used. Applying for fixed support on the pin support hence the rotating disc is fixed with the shaft, give the rotating disk an angular velocity at 1 second 382 rad/s and become zero in 2.5 second in the z-direction, and import the temperature load which causes stress due to temperature on the nodal elements.

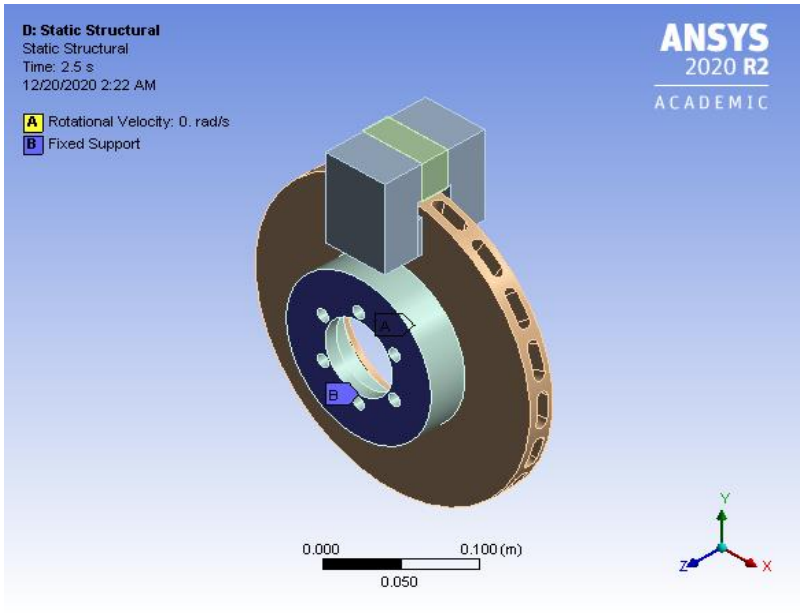

Figure 3.32: Loading and boundary condition of steady-state thermal analysis

The temperature results from the thermal analysis are imported to the structural analysis at the boundary conditions of atmospheric temperature as shown in Figure 3.33 noting the maximum temperature is red colored areas and the lower temperature is represented in blue.

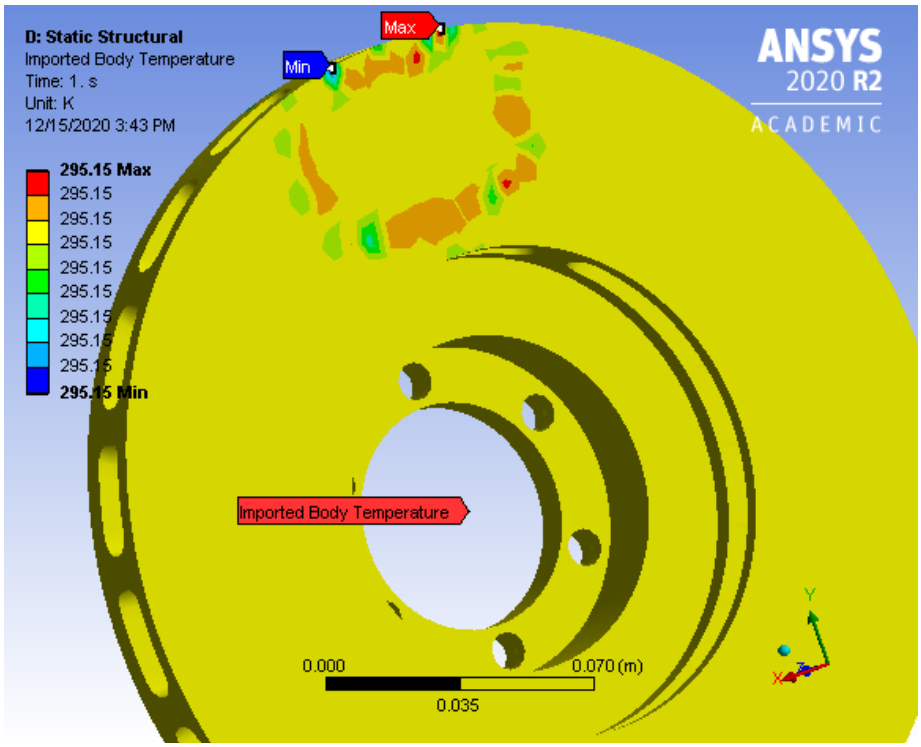

Figure 3.33: Imported body temperature load

Static structural analysis proved the solution of:

- Directional and total deformation.
- Components, principal, or invariants of stresses and strains.
- Contact output.
- Reaction forces

Chapter Four

4. Result and Discussion

4.1. Result

4.1.1. Magnetostatic Results

An optimized result is obtained by changing the area of the conductor A_c, $6.78\,x\,10^{-9}m$ and number of turn N, 97 turns from numerical analysis to $9.6\,x\,10^{-6}m$ and 70 turns respectively show better results in magnetic coenergy and torque. Figure 4.1 shows, the different colors represent different magnetic field fluxes. The area closer to the magnetic coil is red, which indicates a maximum B. The B of other areas continually decreases farther away from the loop and is represented by blue.

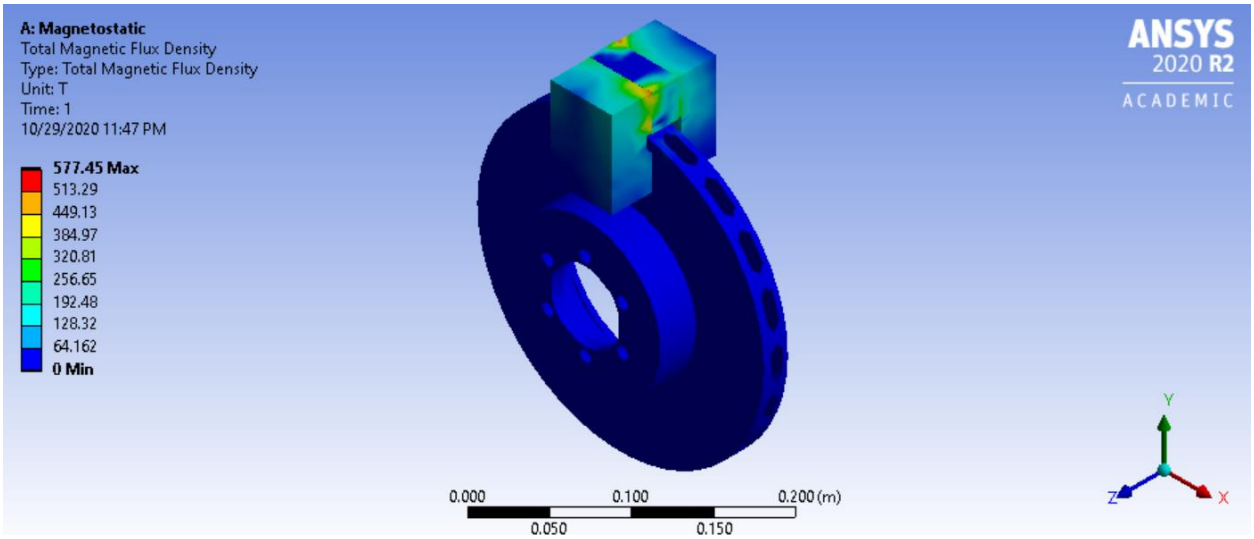

Figure 4.1: Total magnetic flux

4.1.2. Thermal Results

From the thermal steady-state analysis, the heat transfer is obtained from convection and radiation therefore the area perpendicular to the magnetic pole gets high heat. As in Figure 4.2, the maximum temperature of the disc area exposed to the core is $904.34K$ this shows the simulation positive result with the numerical analysis result of energy conversion $914.29K$. hence the disc material is aluminum and can withstand till maximum temperature that $973.15K$.

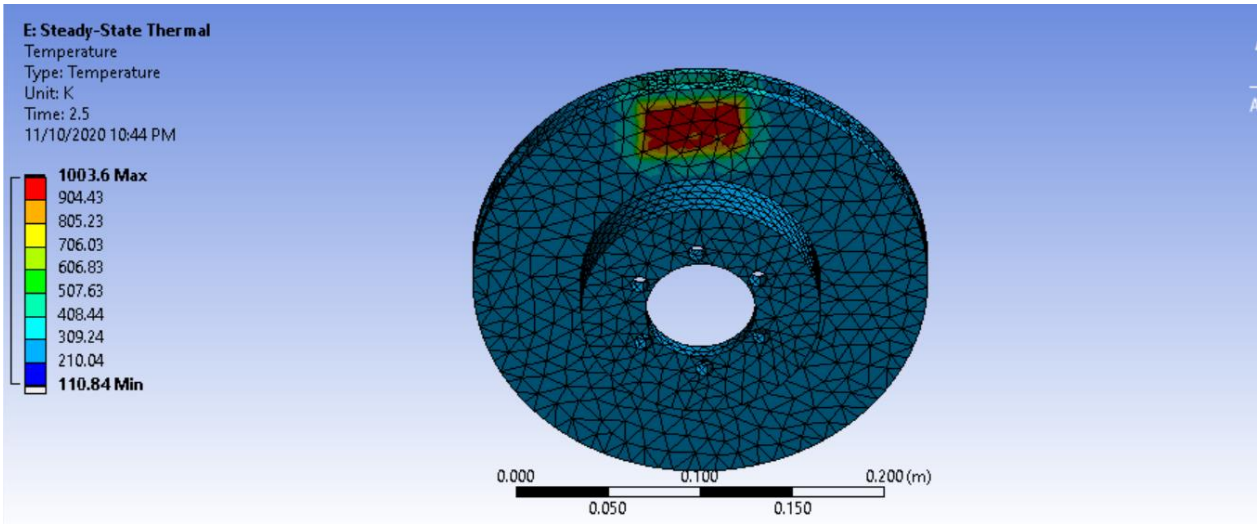

Figure 4.2:Temperature distribution on the disk

The result for total heat flux and directional heat flux towards the axis of rotation as presented in Figure 4.3 and Figure 4.4 the maximum heat flux created by the magnetic field to stop the rotating disk from angular speed 382 rad/s is $2.181x\ 10^7\ w/m^2$ and $1.6\ x\ 10^7\ w/m^2$ respectively.

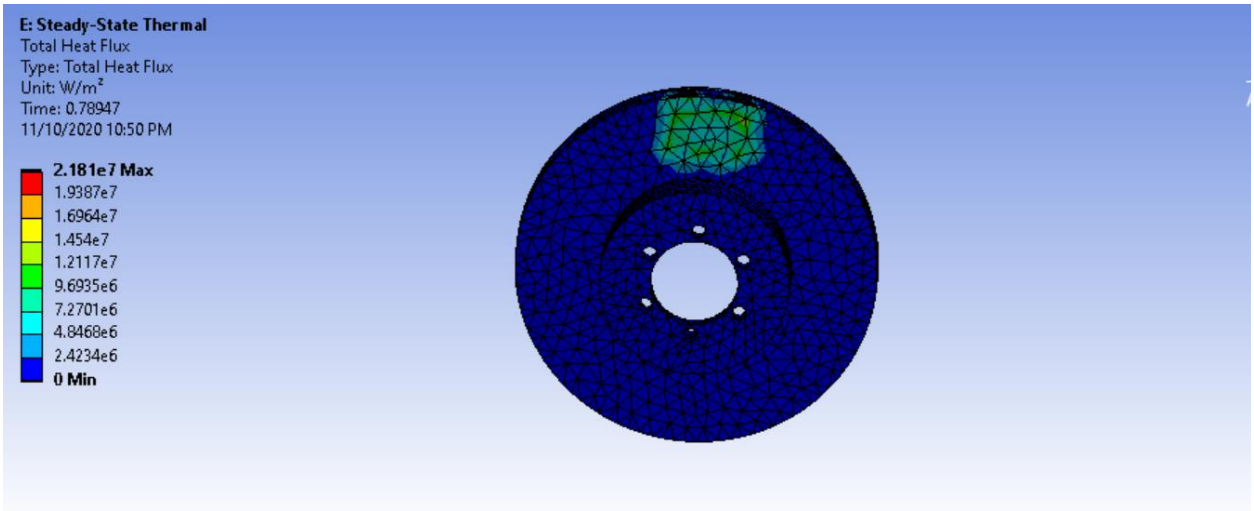

Figure 4.3: Total heat flux distribution on the disk

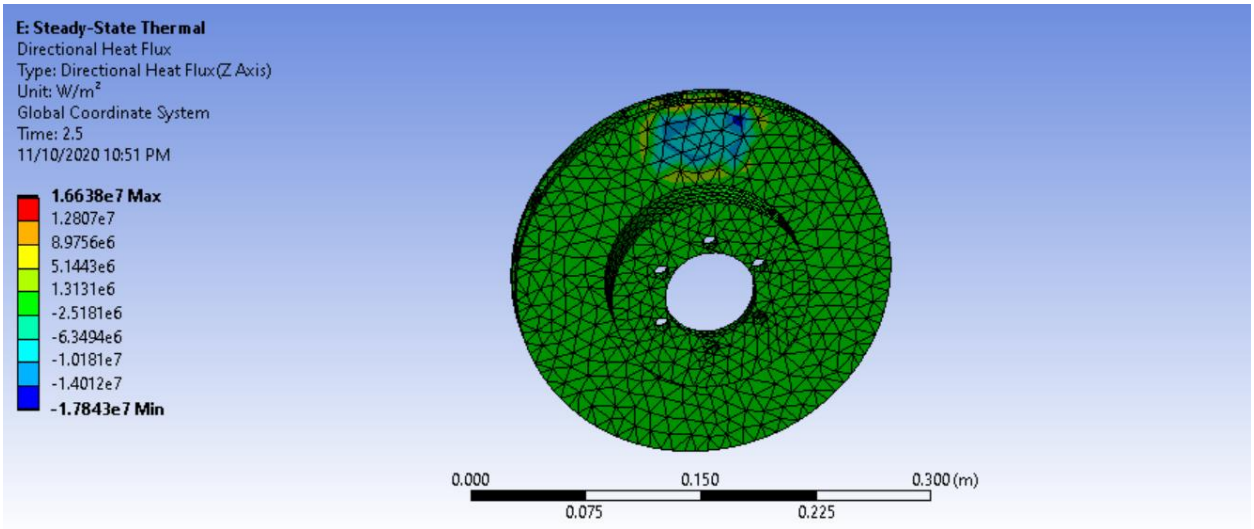

Figure 4.4: Directional heat flux in the z-direction

4.1.3. Structural Results

From the simulated result, in Figure 4.5 the thermal stress on a disc surface at the disc effective radius is illustrated the maximum value of von Mises stress created due to temperature load is 16MPa, the disc is safe from failure hence the yield strength of aluminum is 276MPa.

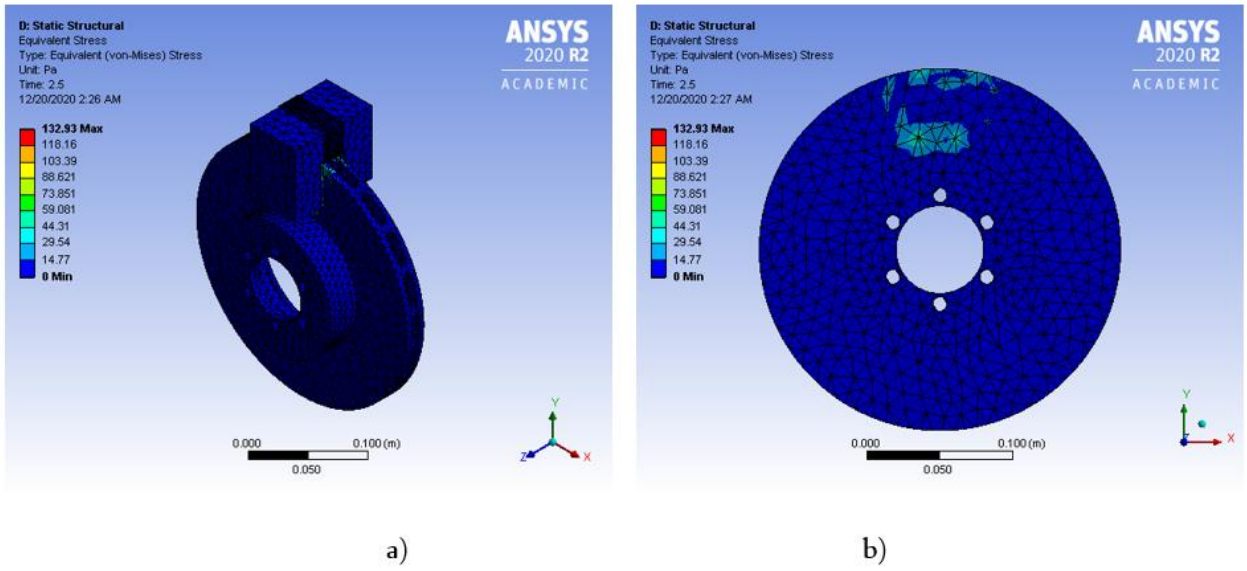

Figure 4.5: Equivalent (Von-Mises) stress simulation results from a) stress distribution on the whole braking system and b) stress distribution on the rotating

The thermal strain ε_0 is determined by the material's thermal expansion coefficient and temperature change. The thermal expansion coefficient $\boldsymbol{\alpha}$ of aluminum is $2.3\ x\ 10^{-5}\ 1/℃$.

$$\varepsilon_T = \boldsymbol{\alpha \Delta T}$$

where the temperature difference $\boldsymbol{\Delta T}$ on the disc is 609.19 K (336.04℃). therefore, the maximum thermal strain ε_T that can endure by the disc is 0.0077 m/m . the maximum equivalent strain created due to thermal stress on the rotating disc Figure 4.6 is 1.9921 x $10^{-9} m/m$ *F*rom this is concluded that the disc is in safe design.

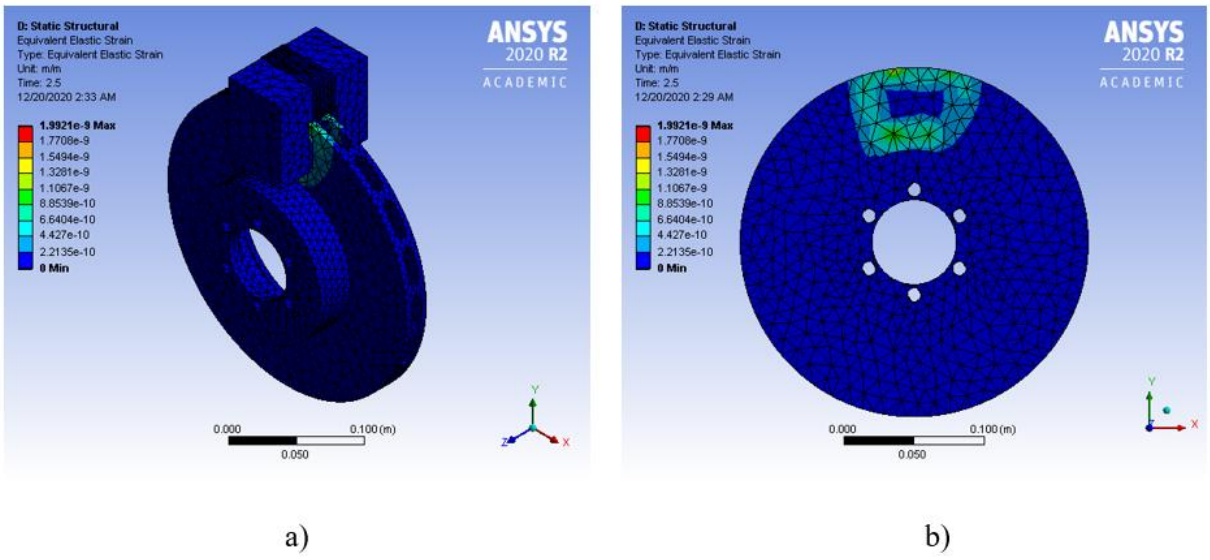

a) b)

Figure 4.6: Equivalent strain simulation results in a) strain distribution in the entire system and b) strain distribution on the rotating disc

The maximum deformation Figure 4.7 is created on the disc is 1.0471 x10^{-11}m.

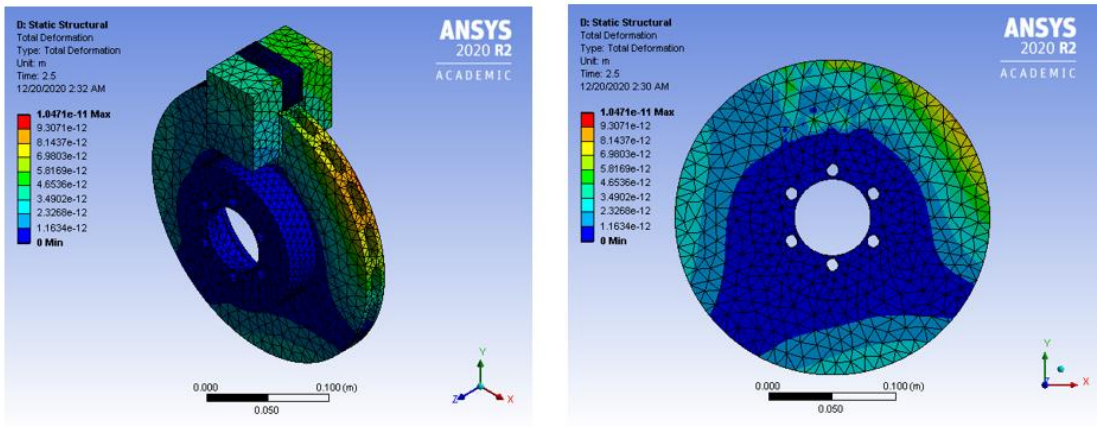

a) b)

Figure 4.7: Total deformation simulation results in a) total deformation on the entire braking system and b) deformation of the rotating disc

4.2. Discussion

A numerical analysis was carried out mechanical analysis on the vehicle quarter model calculation to obtain the data in the form of braking torque generated under various assessed conditions by the electromagnetic brake system. Through electrical analysis, the features of the variables leading to the optimal brake design are determined through the use of the data. The magnitude of the magnetic field, which influences the conductor or the magnetic flux density of the air gap, is determined by applying the computed braking torque. Therefore, the electromagnetic brake system is designed for an optimized result obtained using Finite element analysis on Ansys software on magnetostatic analysis by changing the area of the conductor A_c, $6.78\ x\ 10^{-9}m$ and number of turn N, 97 turns from numerical analysis to $9.6\ x\ 10^{-6}m$ and 70 turns respectively show better results in magnetic co-energy and torque to stop the vehicle at 2.5 seconds. The calculated numerical values of vehicle dynamics were also validated on MATLAB software (Appendix IV) the result in Figure 4.8 shows agreement except for minor differences that created inaccurate calculations manually.

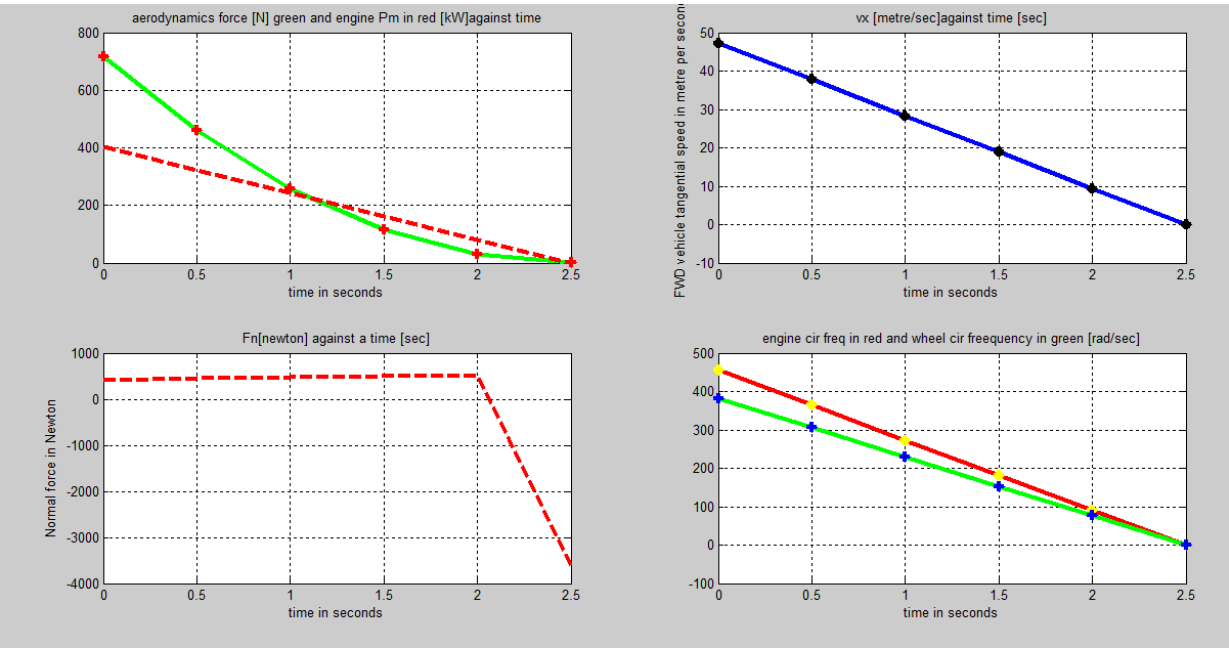

Figure 4.8 Electromagnetic performance test using Matlab

The relation between braking torque produced by the electromagnetic brake system and the angular speed of the conducting disc is compared using calculation, MATLAB, and ANSYS software Table 4.1. The simulation result on the relation between torque produced by the electromagnet and the angular speed of the disc is linear at low speed and nonlinear at high speed as shown in graph Figure 4.9. which shows a parabolic future as the speed goes higher while the calculated result is linear. This occurs because relying only on mathematical analytics leads to an imprecise computation as it ignores object geometry, software library input settings, and datasheet variance. Conversely, the FEM analysis yields results that are in good agreement with actual conditions because it considers the geometry of the object and analyzes the model on a ventilated disc, whereas the numerical analysis considers a solid disc to reduce computational complexity.

Table 4.1: Comparison of braking torque created by the electromagnetic brake system

Angular Speed (rpm)	Braking Torque(Nm) calculation	Braking Torque(Nm) MatLab	Braking Torque(Nm) *ANSYS*
100	7.486415285	14.12	16.678
500	37.43207642	53.23	64.67
1000	74.86415285	120.657	138.344
2000	149.7283057	223.5	250.358
3000	224.5924585	250.451	313.127
4000	299.4566114	273.932	338.012

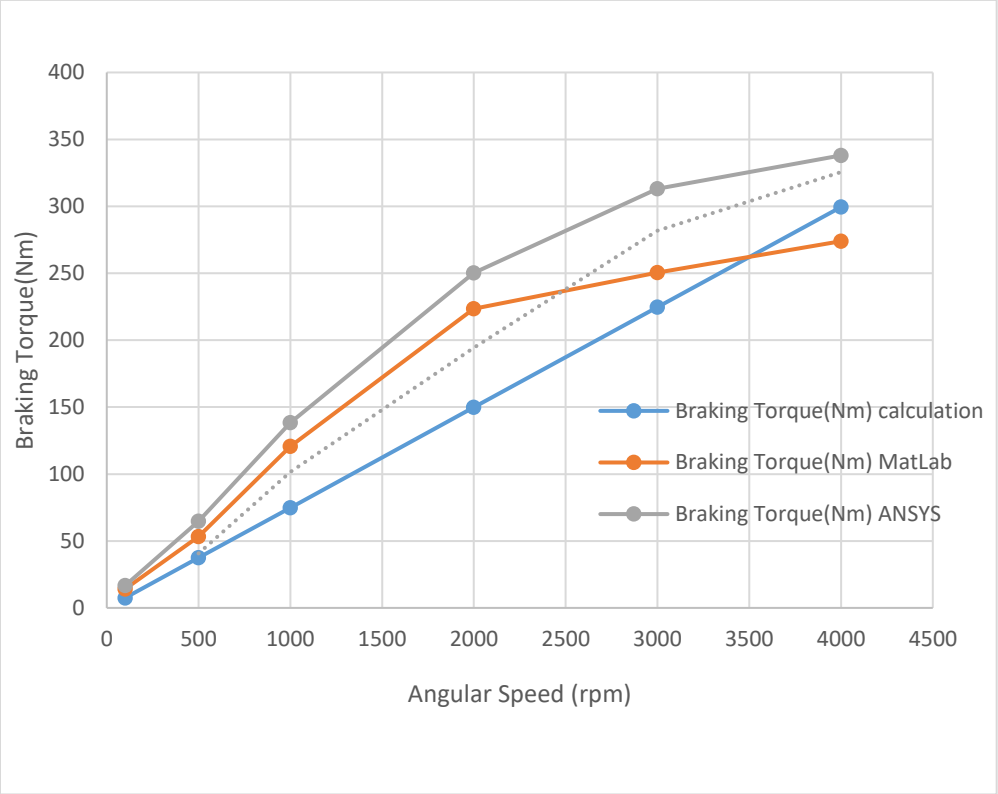

Figure 4.9: braking torque vs Angular speed of EMB

From Figure 4.9, the braking torque at a high speed of 4000 rpm is higher than at a lower speed 500rpm this happened due to core loss at lower speeds but when it goes higher than 4000rpm it tends to drop this can be improved by regulating the current during lower speed. the magnetic field in Figure 4.1 is concentrated at the area of the conducting disc where it is exposed to the magnetic field only. These are caused by the skin effect as the thickness increases skin effect increases and leads to a decrease in torque. this problem can be solved by improving the material quality as well as improving the conducting disc structure by creating fins at the surface to help create more air gaps to reduce the skin effect.

Chapter Five

5. Conclusion and future work

5.1. Conclusion

In this thesis work, an electromagnetic brake (EMB) design has been presented as a competitive substitute for the existing conventional hydraulic brake (CHB) system for a lightweight vehicle Lifan 530. Theoretical analysis and numeric assumptions have been done to obtain braking torque and electromagnetic components parameters. the EMB components are designed with a focus on the optimization of the magnetic circuit and selection of material to stop the vehicle in 2.5 seconds using a 12v battery without needing an extra battery power source. Using ANSYS Workbench 2020 R2, a 3D finite element model of the EMB was created by SpaceClaim 2020 R2 to simulate and optimize the EMB domain using magnetostatic analysis to study the magnetic flux and braking torque created by the system. Steady-state thermal analysis was performed to investigate heat buildup and the thermal effect of the electromagnet on the brake system. Moreover, to study the structural response to the temperature effect a static-structural analysis is performed. To optimize the magnetic circuit design to maximize the braking torque FEM is used. The ANSYS magnetostatic solver is built with an algorithm to optimize by changing the conductor area and the number of turns. therefore, the optimized electromagnetic result is achieved by the wire diameter of 3.2×10^{-4}m and 70 turns. The simulated result presented that the braking torque increased with the conducting area. The generated braking torque by the EMB is compared using the calculation, MATLAB, and ANSYS with the angular speed of the conducting disc the result shows the braking torque is higher at the higher speed. therefore we can conclude that the designed EMB system can replace the CHB in Lifan 530 by regulating the excitation current during lower and higher speeds without adding an extera battery.

5.2. Future Work

In future work, to achieve the ideal design and performance of the electromagnetic brake system (EMB) in connection to several criteria, research connected to efforts to clarify how the EBM system may effectively stop vehicles is necessary. This paper recommends further study as follows;

- Occupant safety for electromagnetic brake system
- Studying the communication network, energy supply system, and braking system redundancy design the safety and reliability of the electromagnetic brake system.
- New composite material can be redeveloped for core magnetic material to reduce the core loss
- Improving structural configuration of conducting disc for EMB to reduce the skin effect.
- A new mathematical model can be developed for EMB that reduces the influence of the angular speed of the conducting disc on braking torque.

References

[1] N. Jackson, "Weebly," [Online]. Available: http://teacherengineer.weebly.com/braking-systems.html. [Accessed 18 December 2023].

[2] Hedrick J.K., Tomizuka, Masayoshi, Varaiya, Pravin, "Control Issues in Automated Highway," *Control Systems, IEEE,* vol. 14, no. 21, p. 32, 1995/01/01.

[3] R. He, C. L. and N. L. , "Fuzzy control of the integrated system of electromagnetic brake and friction brake of car," *Journal of Mechanical Engineering,* vol. 46, no. 24,, p. 83–87, 2010.

[4] J. Kukutschová, R. V, M. K, P. Z, H. R, K. J., M. V, M. D and F. P, Wear Mechanism in Automotive Brake Materials, Wear Debris and Its Potential Environmental Impact, Carbondale, IL, 62901-4343 US: Southern Illinois University Carbondale, Centre for Advanced Friction Studies, 2009.

[5] O. Uexkull, S. S. R. D. and M. B. , "Carbide Antimony inbrake pads a carcinogenic component," *J. Cleaner Prod,* no. 13(2005), pp. 19-31, 2005.

[6] R. A. Peters, "Environmental Effects of Copper in Brake Pad Wear Debris,," in *Brake Pad Partnership Brake Colloquium & Exhibition.*, 2008.

[7] k. Nice, "http://www.workhowstuffworks.com," 12 2011. [Online]. Available: how power brakes(200-08-22). [Accessed 6 2017].

[8] K. K.Lee, "Environmental Optimal Robust Control of a Contactless Brake System Using an Eddy Current," *Journal of Mechatronics,* vol. 9, no. 6, p. 11, 1998.

[9] S. C. B. Umang S. Modi, "Current trends in Electro-magnetic Braking System: A review paper ofthe current scenario of the magnetic braking system," *International Journal for Scientific Research & Development|,* vol. 3, no. 06, pp. 1-4, 2015.

[10] L. Cadwell, "Magnetic damping: Analysis of an eddy current brake using an air track," *American Journal of Physics,* vol. 64, no. 7, pp. 917-923, 1996.

[11] P. N.B.Totala, P. B. S. J. S. J. and K. K. , "electromagnetic braking system," in *National Conference on Innovations in Mechanical Engineering*, pune41205,india, 6-8 April 2015.

[12] R. He, X. L. and C. L. , "Brake Performance Analysis of ABS for Eddy Current and Electrohydraulic Hybrid Brake System," in *Mathematical Problems in Engineering*, Hindawi Publishing Corporation, 2013, p. 11.

[13] K. Karakoc, E. J. P. and A. S. , "Design considerations for an automotive magnetorheological brake," *Mechatronics,* pp. 1-14, 22 February 2008.

[14] K. K. E. J. P. and A. S. , "Improved braking torque generation capacity of an eddy current brake with time varying magnetic fields: A numerical study," *Finite Elements in Analysis and Design,* vol. 59, pp. 66-75, 23 september 2012.

[15] S. P, N. K. V. and M. M. S. , "Innovative Electro Magnetic Braking System," *International Journal of Innovative Research in Science, Engineering and Technology,* vol. 3, no. 2, pp. 46-53, April 2014.

[16] S. D. S. S. A. S. a. A. R. S. Dr. S. R. Pawar, "Analysis of Electromagnetic Braking System," *IJRES,* vol. 10, no. 4, pp. 19-26, 2021.

[17] T. M and M. N. H., "Use of Finite Element Method for the Numerical Analysis of Eddy Current Brake," *Journal of Electrical Engineering,* vol. 15, no. 1, pp. 121-126, september 2015.

[18] M. . M. G. and . S. , "EDDY CURRENT BRAKING STUDY FOR BRAKE DISC OF ALUMINIUM, COPPER AND ZINK," in *Regional Engineering Postgraduate Conference (EPC*, 2011.

[19] M. Dekker, Magnetic materials and their characteristics, 2004.

[20] j. moser, "electromagnetic devices for operation in high temperature ambient of 1000oF(500OC)," Firstmark aerospace, july 1 2003.

[21] K. Lee, K. P. J. K. and a. S. Wang, "Torque analysis and optimization of aneddy current brake system," San Jose, CA, USA, Proc. of IMCSD 99, 1999, p. 137–141.

[22] Li Luo, Qingzhi Zhai, Wen Li, Chen Qian,Hong Liu, "Research on an Integrated Electromagnetic Auxiliary Disc Brake Device for Motor Vehicle," *IEEJ TRANSACTIONS ON ELECTRICAL AND ELECTRONIC ENGINEERING,* no. IEEJ Trans 12, p. 434–439, 2017.

[23] M.-P. Todor1, "SYSTEMATIC APPROACH ON MATERIALS SELECTION IN THE AUTOMOTIVE INDUSTRY FOR MAKING VEHICLES LIGHT MORE FUEL–EFFICIENT," *Applied Engineering,* vol. 1, no. 2466-4847, pp. 91-97, 2016.

[24] M. Yu, Aluminium cables in automotive applications, STOCKHOLM, : KTH, 2016.

[25] "Selection Of Electrical Steels For Magnetic Cores," AK Steel Corporation, 2007. [Online]. Available: https://www.brhttps://www.brown.edu/Departments/Engineering/Courses/ENGN1931F/mag_cores_dataAKSteel-very%20good.pdf.

[26] F. Fausto, "Measurement and Characterization of Magnetic Materials," *Elsevier Academic Press,* 2004.

[27] X. C. Y. L. C. M. J. C. Gaoyuan Ouyang, "Review of Fe-6.5 wt%Si high silicon steel—A promising soft magnetic material for sub-kHz application," *Journal of Magnetism and Magnetic Materials,* vol. 481, pp. 234-250, 2019.

[28] "Chapter A: Wire Bonding 2 Level 2. Conclusions and guideline," University of Florida.

[29] W. yung, Theory of Ground Vehicles,Third Edition, United States of America: Wiley-Interscience, ISBN 0-471-35461-9, 2001.

[30] W. H. Y. and A. W. Y. , Handbook of small electric motors, USA: McGraw-Hill, 2003.

[31] *gear ratio for 5MT continuously variable transmition (CVT).* [Performance]. Subaru motor vehicles, 2012.

[32] P. Jun Cui, Writer, *Low Loss Soft Magnetic Materials for Industrial Motor.* [Performance]. the Ames Laboratory creating materials and energy solution.

[33] S. M. S. ·. M. Tanelli, Active Braking Control Systems Design for Vehicles, Springer London Dordrecht Heidelberg New York: Springer, July 19, 2010.

Appendix

Appendix I: Data sheet

Table 0.1: Approximate static relative permeability of magnetic materials [19]

Material	Class	Relative permeability (μ_{sr})
Bismuth	Diamagnetic	0.999834
Silver	Diamagnetic	0.99998
Lead	Diamagnetic	0.999983
Copper	Diamagnetic	0.999991
Water	Diamagnetic	0.999991
Vacuum	Nonmagnetic	1.0
Air	Paramagnetic	1.0000004
Aluminum	Paramagnetic	1.00002
Nickel chloride	Paramagnetic	1.00004
Palladium	Paramagnetic	1.0008
Cobalt	Ferromagnetic	250
Nickel	Ferromagnetic	600
Mild steel	Ferromagnetic	2,000
Iron	Ferromagnetic	5,000
Silicon iron	Ferromagnetic	7,000
Mumetal	Ferromagnetic	100,000
Purified iron	Ferromagnetic	200,000
Supermalloy	Ferromagnetic	1000,000

Table 0.2: Thermal conductivity of other common metals used in auto-industry [18]

Rank	Metal	Thermal Conductivity [BTU/ (hr.· ft·°F)]
1	Copper	223
2	Aluminum	118
3	Brass	64
4	Steel	17
5	Bronze	15

Table 0.3: the resistivity and temperature coefficient at 200c for some common materials.

Material	**Resistivity (ohm-m)**	**Temperature coefficient α(/^{0}c)**	**Conductivity σ 10^7/Ωm**
Silver	1.59 x10^{-8}	0.0038	6.29
Copper	1.68 x10^{-8}	0.00386	5.95
Copper, annealed	1.72 x10^{-8}	0.00393	5.81
Aluminum	2.65 x10^{-8}	0.00429	3.77
Tungsten	5.6 x10^{-8}	0.0045	1.79
Iron	9.71 x10^{-8}	0.00651	1.03
Platinum	10.6 x10^{-8}	0.003927	0.943
Manganin	48.2 x10^{-8}	0.000002	0.207
Lead	22 x10^{-8}		0.45
Mercury	98 x10^{-8}	0.0009	0.10
Nichrome (Ni, Fe, Cr alloy)	100 x10^{-8}	0.0004	0.10
Constantan	49 x10^{-8}		0.20
Carbon(graphite)	3-60 x10^{-5}	-0.0005	
Germanium	1-500 x10^{-3}	-0.05	
Silicon	0.1-60	-0.07	
Glass	1-10000 x10^{9}		

Table 0.4: Comparison of properties of aluminum and copper.

Property	Aluminum	Copper (OF grade)
Purity	99.7%	99.95%
Resistivity	28.3nΩm	17.2 nΩm
Thermal resistivity coefficient	0.004k^{-1}	0.004k^{-1}
Density	2.70 kg/dm^3	8.94 kg/dm^3
Thermal conductivity	237w/m k	391 w/m k
Approx. price	4.7€/kg	11€/kg

Table 0.5: Gear ratio for 5MT continuously variable transmission(CVT) [31]

Gear shift	Gear ratio
1st gear	3.454

2nd gear	1.888
3rd gear	1.296
4th gear	0.972
5th gear	0.738
Final drive	4.11
Reverse gear	3.333

Table 0.6: SOA soft magnetic materials [32]

Type	Material	Bs (T)	Hc (A/m)	10^3 μ_r 1KHz	R ($\mu\Omega$ – cm)	λ(ppm)	$W_{1.5/50}$ (W/kg)	$W_{10/40}$ (W/kg)
Crystalline	Electrical steel,3.2% Si	2	26	15	57	8	0.7-1.2	11
	Electrical steel,6.5 % Si	1.4	45	19	82	0.01	0.6	8.1
	Molypermalloy $Ni_{78}Fe_{17}Mo_5$	0.65-0.82	0.25-0.64	100-800	60	2-3	0.07	0.3
	Hipercop50, $Fe_{49}Co_{49}V_2$	2.4	16-400	5-50	27	60	4	10
Nano-crystalline	Finemet, $Fe_{73.5}Si_{13.5}Nb_3B_6Cu_1$	1.2	0.5-1.4	80	110	0-2	--	1.1
	Nanoperm, $Fe_{88}B_4Zr_7Cu_1$	1.5 - 1.6	2.4-4.5	48	56	0	--	3
	Hitperm,$(FeCo)_{44}Zr_7Cu_1$	1.6-2.0	80-200	1-10	120	36	--	20
Amorphous	Metglas, $Fe_{78}Si_9B_{13}$	1.54	3	2.1	135	27	0.7	2-5
	Metaglas 2650Co, $Fe_{67}Co_{18}B14Si$	1.8	3.5	50	123	35	0.3	3
Ferrite	Ferrite, MnZnFeO	0.36 -0.5	10 -100	0.5-10	10^7 - 10^8	5	--	--
	Ferrite, NiZnFeO	0.25 -0.42	14-1600	0.01 -1	10^{11}	-20	--	--

Appendix II: Graphical data inputs

Graph 1 Friction coefficient versus slip ratio for different road surfaces [33]

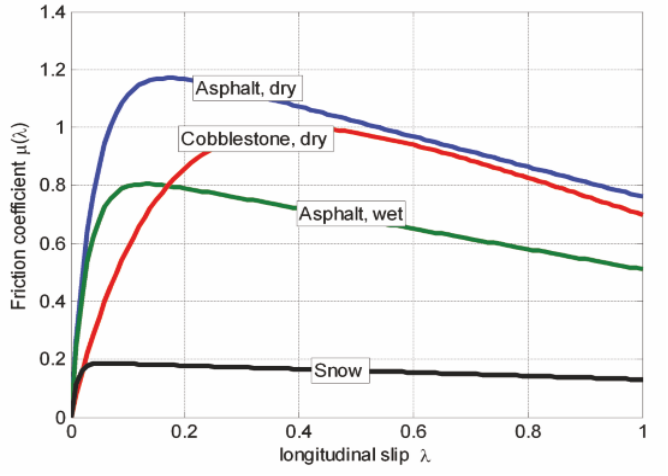

Graph 2 FeSi wt 3.2% BH curve from ANSYS library

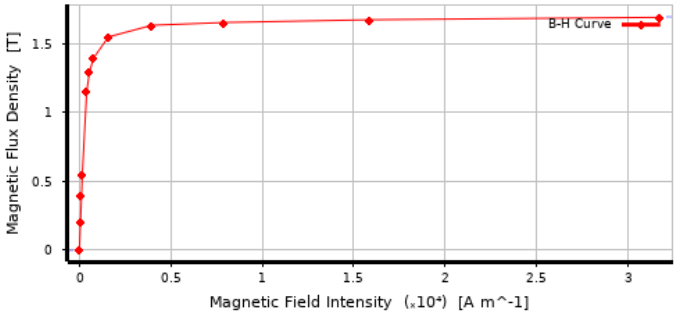

Graph 3 Magnetic material hysteresis loop and characteristic parameters [29]

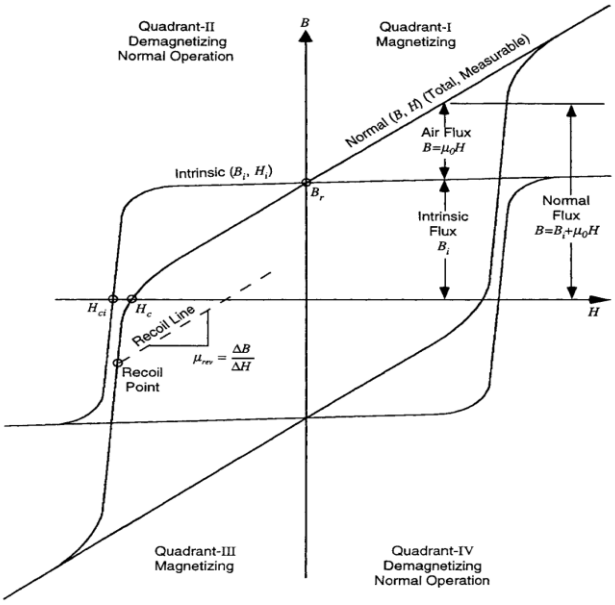

Appendix III: Model description on ANSYS workbench

TABLE 4
Model (A4, B4) > Geometry > Part > Parts

Object Name	*Air*	*core magnet*	*coil*	*hub sit*	*rotating disk*
State	Hidden	Meshed			
Graphics Properties					
Visible	No	Yes			
Transparency		1			
Definition					
Suppressed	No				
Stiffness Behavior	Flexible				
Coordinate System	Coordinate System	Default Coordinate System	Coordinate System	Default Coordinate System	
Reference Temperature	By Environment				
Treatment	None				
Material					
Assignment	Air	iron silicon 3.2 % si	Aluminum silicon 1 % si	Aluminum Alloy	
Nonlinear Effects	Yes				
Thermal Strain Effects	Yes				
Bounding Box					
Length X	0.347 m	5.3e-002 m	5.42e-002 m	0.13 m	0.247 m
Length Y	0.347 m	7.42e-002 m	3.12e-002 m	0.13 m	0.247 m
Length Z	0.1205 m	9.e-002 m	2.3e-002 m	3.05e-002 m	2.05e-002 m
Properties					
Volume	1.3537e-002 m³	2.9558e-004 m³	1.1702e-006 m³	2.4431e-004 m³	4.3075e-004 m³
Mass	1.6583e-002 kg	2.2169 kg	3.1596e-003 kg	0.67675 kg	1.1932 kg
Centroid X	-2.1264e-005 m	9.8e-004 m		-2.8357e-006 m	-5.17e-006 m
Centroid Y	-0.1604 m	-3.4425e-002 m	-1.5e-002 m	-0.1577 m	
Centroid Z	-9.3563e-004 m	-4.4369e-004 m	-4.3e-004 m	2.6286e-002 m	5.9299e-005 m
Moment of Inertia Ip1	1.9036e-004 kg·m²	2.8158e-003 kg·m²	7.1033e-007 kg·m²	1.027e-003 kg·m²	6.3449e-003 kg·m²
Moment of Inertia Ip2	1.9623e-004 kg·m²	2.2867e-003 kg·m²	1.4618e-006 kg·m²	1.0276e-003 kg·m²	5.6018e-003 kg·m²
Moment of Inertia Ip3	3.4469e-004 kg·m²	1.5669e-003 kg·m²	1.8935e-006 kg·m²	1.9464e-003 kg·m²	1.1823e-002 kg·m²
Statistics					
Nodes	25057	2124	594	1963	6290
Elements	15041	1147	108	983	3005
Mesh Metric	None				

Model (A4) > Magnetostatic (A5) > Commands (APDL)

```
!   Commands inserted into this file will be executed just prior to the ANSYS
SOLVE command.
!   These commands may supersede command settings set by Workbench.

!   Active UNIT system in Workbench when this object was created:  Metric (m,
kg, N, s, V, A)
!   NOTE:  Any data that requires units (such as mass) is assumed to be in
the consistent solver unit system.
!                See Solving Units in the help system for more information.
```

Appendix IV: Mathlab coding

```
%the following is a code for car braking
%mechanical part is modelled using linear car motion. the motion is modelled
% assuming the breaking is happened linearrly.
%_____________________________________________________________________________
t=0:0.5:2.5;% time taken for vehicle to be braked
pi=3.1428; % greek pi value from ancient Babylonians
H=1; %tilted height of car in metre
vx=-18.8888.*t+47.22; %longtudinal in metre pr seconds
acc=2*diff(vx);% decelaration
Lbase=2.55; %base length in metre
Rw=0.1235;% wheel radius in metre
Te=119;% maximum driving or engine torque in Nm at maximum speed 47.22ms^-2
gearratio=0.84;% Lifan 530 5th gear ratio
Ww=vx/Rw;% wheel circuklar speed in rad per second. It is 3605rpm
Theta=asind(H/Lbase); %tilt angle
%_____________________________________________________________________________
mv=1515;%curb mass of vehicle in kg
msw=8.5;% mass of sigle wheel in kg
g=9.81;% gravitational accelaration in gram per seconds
fzrprime=1694.5;% in N
fzr=587.5; %in N
hcg=0.5*(((fzrprime-fzr)*Lbase)/(mv*g)+(tand(Theta))+Rw);%centre of gravity
mt=0.25*mv+msw;
rho=1.225; %mass density of air in kgm^-3
cd=0.26;%air drag coefficient
Af=1.6+0.00056*(mv-765);% frontal car area given in literature 30
Faero=0.5*rho*cd*Af*vx.*vx; % in Newton
%_____________________________________________________________________________
Lr=0.5*Lbase;
Fn=[mt*g mt*g mt*g mt*g mt*g mt*g]-([mv*g*Lr mv*g*Lr mv*g*Lr mv*g*Lr...
    mv*g*Lr mv*g*Lr]+[mv*hcg.*acc 0]+Faero.*hcg)*(1/Lbase);
%_____________________________________________________________________________
Cr=0.01.*([1 1 1 1 1 1]+vx.*3.6/147);%rolling coeffeicient
Rx=Cr.*[Fn(:,1) Fn(:,2) Fn(:,3) Fn(:,4) Fn(:,5) 0]; %rollimg resistance
s=(4000*2*pi*Rw/60)/(vx(:,1))-1;%slip coefficient
%at s=0.1 friction corfficient is approximately 1 from graph
```

```
mu=1; %friction coefficient
Ff=mu*Fn;% force of friction in N
Iw=0.5*msw*Rw.*Rw;%wheel inertia in kgm^2
We=Ww/gearratio;%Wheal circular freequency in rad per seconds or 4946rpm
Tl=(-6.744+28.8-20.4477).*10^(-6)*We(:,1).*We(:,1);% load torque in Nm
alphae=2*diff(We); %constant engine accelaration
Ie=-(Te-Tl)/alphae(:,1); % engine enertia in kgm^2
I=Iw+(1/(gearratio)^2)*Ie;% effective mass enertia
%_____________________________________________________________________
Alphawheel=2*diff(Ww); %Wheel decelaration
Tb=Te+Rw.*(Rx(:,1)-Ff(:,1))-I*Alphawheel(:,1); %mechanical braking torque
%at 0second_____________________________________________________________

%The following is the design of electrical parts using the above braking
%torque. In this section electrical paramrtres are to be designed
B=0.141; %magnetic flux for magnetic iron core sellected in Wb/m
dens=2712; %standard density of aluminium disk in kgm^-3
d=0.0205;% standard disk thickness in metre
cond=3.5*10^7;% aluminium core conductivity in siemens/metre
D=sqrt(4*Tb/(pi*d*cond*B^2.*(Rw)^2.*Ww(:,1)));% Diagonal of disk
%by taking the the diagonal angle to be 30 degree
thetha=30;
a=D*cosd(thetha);%core width in metre
b=D*sind(thetha);% magnetic core crossection height
Wcore=b;% Width of the core in metre
Acore=a*b;% magnetic cross section area in m^2
%the following is to calculate amagnetic path length MPL
%_____________________________________________________________________
syms Pc Ph Pe Ue Um i
Pc=Ph+Pe;
%Ph=(2/3)*Pc;
Bs=1.5; %maximum field in T at Pc loss of 0.7w/kg
Hc=26; %hysterisys loss at 1.5T and 50Hz in At/m
f=50; % freequency
FeSirho=7800;%iron silicon core in kgm^-3
Ph=4*Bs*Hc*f/FeSirho;
Pcloss=0.7; %in w/kg
Mcore=1.5*Ph/Pcloss;% Mcore=Vvol*FeSirho=MPL*Acore*FeSirho in kg
```

```
MPL=Mcore/(Acore*FeSirho);%in metre
Lcore=0.25*MPL+2*b-0.56*b;% lenth of the core in metre
Lwindow=Lcore-2*Wcore; %in metre
mu0=4*pi*10^(-7); %air permibility in H/m
mur=15000; % relative  permitivity
Lairgap1=0.001; %length of airgap one inmetre
Lairgap2=Lairgap1;
Aairgap1=Acore;%area of air gap one
Aairgap2=Acore;
Alcond=Acore;% disk area exposed to magnetic flux
FeSiAcore=Acore;
%the total reluctance on the system in AT/Wb is
Rtot=MPL/(mu0*mur*FeSiAcore)+Lairgap1/(mu0*Aairgap1)+d/(mu0*Alcond)+....
    Lairgap2/(mu0*Aairgap2);
%the following section is used to find the coil length and number of turns
%_____________________________________________________________________
%the energy balance is supposed to be maintained while converting
%Um=Ue.........0.5Li^2=Utrans+Urotat
%L=(mt*vx.*vx+0.5I.*Ww.Ww)/i^2
%the mechanical power developed due to wheel is given by
Pm=-(mt*vx.*[acc 0]+I*Ww.*[Alphawheel 0]); %in 10w
V=12; % a 12volt battry
i=Pm(:,1)/V;% maximum eddy current magnitude in the magnetic loop  in Ampre
Um=(0.5*mt*vx.*vx+0.5*I*Ww.*Ww); % mechanical energy formed while bracking
L=2.*Um(:,1)/(i(:,1).*i(:,1)); % the maximum or worst case is to be
considered
%while designing an inductor given in Henry
N=sqrt(L*Rtot); %number of turns to be used
lmeancoil=N^2*mu0*Acore/L;% mean turn length of coil in metre
% the resistivity of the wire can be calculated from power loss due to heat
%_____________________________________________________________________
%pl=I^2*R and assumming this power loss is dissipated by heat totally
%Q=Qconvection +Qradiation  over the time interval
h=22.2*1000; %overall heat transfer in w/m^2k
Q=Pm(:,1);
delT=Q/(h*(pi*((Rw)^2-(Rw-0.05)^2)));% in kelvin
Ta=293.15; % room temprature in kelvin
Tmax=delT+Ta;
```

```
%the resistance of the winding is obtained as
Awinding=b*lmeancoil; %in m^2
e=0.09; %emmissivity of the surface
BC=5.67*10^-8; %stefan Boltsmann constant
R=V^2/((h*Awinding)*delT+e*BC*Awinding*(Tmax^4-Ta^4));%in ohm
%The diametre of the wire is
lwire=lmeancoil*N; %length of the wire to be used.
resistAlSi=2.7*10^(-8); % resistivity of aluminium silicon in ohm metre
dwire=sqrt(4*resistAlSi*lwire/(pi*R));% R=resistAlSi*lwire/Awire in ohm
figure (1)
subplot(2,2,1);
plot(t,Faero,'+-g','LineWidth',3,'MarkerEdgeColor','r','MarkerSize',8)
title('aerodynamics force [N] green and engine Pm in red [kW]against time')
xlabel('time in seconds')
hold on
plot(t,0.001*Pm,'--r','LineWidth',3,'MarkerEdgeColor','g','MarkerSize',8)
grid on
subplot(2,2,2);
plot(t,vx,'*-b','LineWidth',3,'MarkerEdgeColor','k','MarkerSize',8)
xlabel('time in seconds')
ylabel('FWD vehicle tangential speed in metre per second')
title('vx [metre/sec]against time [sec]')
grid on
subplot(2,2,3);
plot(t,Fn,'--r','LineWidth',3,'MarkerEdgeColor','b','MarkerSize',8)
xlabel('time in seconds')
ylabel('Normal force in Newton')
title('Fn[newton] against a time [sec]')
grid on
subplot(2,2,4);
plot(t,We,'-*r','LineWidth',3,'MarkerEdgeColor','y','MarkerSize',8)
title('engine cir freq in red and wheel cir freequency in green [rad/sec]')
xlabel('time in seconds')
hold on
plot(t,Ww,'+-g','LineWidth',3,'MarkerEdgeColor','b','MarkerSize',8)
grid on
%_____________________________________________________________________
hold off
```

```
figure (2)
% the engine torque is supposed to be decreased depending on the
%engine circular frequency
Tbrange=[Te Te Te Te Te 0].*[We(:,1)/We(:,1) We(:,1)/We(:,2)....
    We(:,2)/We(:,3) We(:,3)/We(:,4) We(:,4)/We(:,5) 0]+Rw.*(Rx)....
  -[Ff(:,1) Ff(:,2) Ff(:,3) Ff(:,4) Ff(:,5) Ff(:,6)+3550]-[I*Alphawheel 0];
plot((60/2*pi).*Ww,-Tbrange,'-*b','LineWidth',3,'MarkerEdgeColor','b',....
'MarkerSize',8)
xlabel(' wheel circular speed in rpm')
ylabel('Braking torque in Nm')
legend('Braking Torque variation with respect to wheel circular speed')
grid on
%_____________________________________________________________________
%the following figure shows engine torque variation wrt to engene circular
% speed variation
hold off
figure (3)
plot(60/(2*pi).*We,[Te Te Te Te Te 0].*[We(:,1)/We(:,1) We(:,1)/We(:,2)....
    We(:,2)/We(:,3) We(:,3)/We(:,4) We(:,4)/We(:,5) 0],'--g',...
    'LineWidth',3,'MarkerEdgeColor','b','MarkerSize',8)
xlabel('engine circular speed in rpm')
ylabel('engine torque in Nm')
legend('engine circular speed vs engine torque')
grid on
%end_____________________________________________________________________
```